Journal of Constructional Steel Research 208 (2023) 107973

Contents lists available at ScienceDirect

Journal of Constructional Steel Research

journal homepage: www.elsevier.com/locate/jcsr

Testing, FE modelling and design of pin-ended stainless steel equal-leg angle section columns and beam–columns

Behnam Behzadi-Sofiani, M. Ahmer Wadee *, Leroy Gardner

Department of Civil and Environmental Engineering, Imperial College London, London SW7 2AZ, United Kingdom

ARTICLE INFO

Keywords:
Equal-leg angles
Stainless steel
Physical testing
EC3 design procedure
Columns and beam–columns
Finite element modelling

ABSTRACT

The behaviour and design of pin-ended stainless steel equal-leg angle section members under compression and compression plus minor-axis bending are investigated herein. The studied members are cylindrically pinned about the minor axis. An experimental investigation, including material testing, initial geometric imperfection measurements and physical tests on hot-rolled stainless steel equal-leg angle section members is first presented. Numerical models are developed and validated against the new experimental data. A numerical parametric study is then presented considering both hot-rolled and cold-formed stainless steel angle section columns alongside beam–columns with a wide range of slenderness values. Finally, new design proposals for pin-ended stainless steel equal-leg angle section members under compression and combined compression and minor-axis bending are developed and verified against the results of existing physical experiments, as well as the newly-generated test and numerical results. The proposed design rules are shown to offer substantially more accurate and consistent resistance predictions compared to existing codified design rules. The reliability of the new design provisions, with a recommended partial safety factor $\gamma_{M1} = 1.1$, is verified following the EN 1990 procedure.

1. Introduction

Angle section members are used in a range of structures, such as towers and trusses alongside the bracing systems in buildings and bridges. Even though studies on angles can be traced back to the 1920s [1], their structural behaviour continues to pose both technical and practical challenges with current design provisions in international standards being known to have significant limitations [2–7]. New resistance functions for steel angle section members recently developed within the US [3,8,9] and European [4–7] design frameworks have led to substantial improvements in the consistency and accuracy of their load-carrying capacity predictions. However, little attention has been paid to pin-ended angle section columns under compression within the scope of Eurocode 3. In addition, angles are often loaded eccentrically (e.g. when connected through one leg), such that the point of action does not coincide with the cross-section centroid (see Fig. 1), resulting in the member experiencing combined compression and bending. It is therefore crucial to study their behaviour under combined loading. Recently, Behzadi-Sofiani et al. [4,5] developed new design equations and procedures for fixed-ended steel and stainless steel angle section columns. However, the proposed design method cannot be directly applied to pin-ended angle section columns with slender cross-sections, because of the shift of the effective centroid that arises under compressive loading, resulting in additional eccentricity and hence bending moments. Building on previous work on fixed-ended angle section columns [4,5] and angle section beams [6,7] along with an expression developed to predict the shift of the effective centroid [2], the current aim is to establish a new approach for designing pin-ended stainless steel equal-leg angle section members subjected to compression and combined compression and minor-axis bending suitable for incorporation into EN 1993-1-4 [10]. Moreover, the accuracy and reliability of the proposals are assessed. A review of existing experimental work and previous methodologies for designing equal-leg angle section columns is presented in Section 2. An experimental investigation, involving material tests and tests on 19 austenitic stainless steel equal-leg angle section members – 5 under compression and 14 under combined loading – is described in Section 3. An extensive programme of numerical simulations, conducted using the commercial finite element (FE) software ABAQUS, is then presented in Section 4. The FE models are first validated against the newly-generated and existing physical experiments on stainless steel angle section members, and subsequently utilised to conduct a parametric study for producing additional data across a wide range of slenderness and torsional-flexural to minor-axis

* Corresponding author.
E-mail addresses: behnam.behzadi-sofiani13@imperial.ac.uk (B. Behzadi-Sofiani), a.wadee@imperial.ac.uk (M.A. Wadee), leroy.gardner@imperial.ac.uk (L. Gardner).

https://doi.org/10.1016/j.jcsr.2023.107973
Received 22 December 2022; Received in revised form 6 April 2023; Accepted 23 April 2023
Available online 9 May 2023

Table 1
Summary of existing experiments on stainless steel equal-leg angle section members.

Reference	Boundary conditions	Loading condition	Axis of bending	Manufacturing process	No. of tests
Behzadi-Sofiani et al. [5]	Fixed-ended	Compression	–	Hot-rolling	5
Menezes et al. [11]				Hot-rolling	13
Liang et al. [12]				Hot-rolling	16
Sun et al. [13]				Hot-rolling	10
Sarquis et al. [14]				Hot-rolling	10
Sirqueira et al. [15]				Hot-rolling	18
Filipovic et al. [16]				Hot-rolling	6
Filipovic et al. [17]				Laser-welding	6
Zhang et al. [18]				Cold-forming	16
Zhang et al. [19]				Cold-forming	4
Dobric et al. [20]				Cold-forming	3
Zhang et al. [22]	Pin-ended	Compression	Minor axis	Hot-rolling	12
Zhang et al. [23]				Hot-rolling	12
Filipovic et al. [16]				Hot-rolling	20
Reynolds [21]				Laser-welding	33
Filipovic et al. [17]				Laser-welding	20
Dobric et al. [20]				Cold-forming	8
Behzadi-Sofiani et al. [7]		Bending	Minor axis	Hot-rolling	2
Behzadi-Sofiani et al. [7]			Major axis	Hot-rolling	5
Zhang et al. [19]			Geometric axis	Cold-forming	6
Theofanous et al. [27]			Geometric axis	Laser-welding	4
Total					229

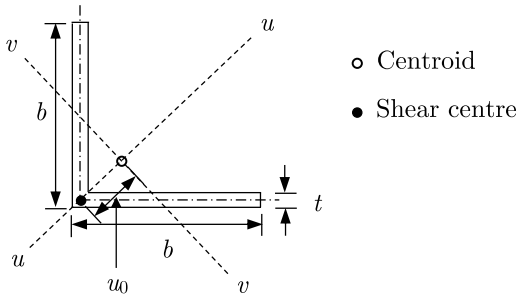

Fig. 1. Dimensions and principal axes of equal-leg angles.

flexural elastic buckling load ratios; the observations are summarised in Section 5. Shortcomings in the current design provisions in EC3 are identified using the experimental and numerical results and are highlighted in Section 6. New proposals for the design of pin-ended stainless steel equal-leg angle section columns and beam–columns are subsequently presented and assessed against the established data. Statistical analyses are performed that confirm the accuracy and reliability of the proposed design method. Finally, conclusions are drawn.

2. Review of previous research

Stainless steel equal-leg angle section columns have been the focus of a number of previous investigations, where their buckling behaviour has been studied under both fixed-ended [5,11–20] and pin-ended [16,17,20–26] supporting conditions. The behaviour of stainless steel angle section members under bending has also been investigated [7,19,27]. Previous tests on stainless steel angle section members are summarised in Table 1, where the manufacturing process, boundary and loading conditions as well as the number of tests are presented. The findings reported in the literature on pin-ended stainless steel angle section columns and beam–columns are described subsequently.

Zhang et al. [22,23] conducted experiments on pin-ended hot-rolled stainless steel angle section columns. Comparisons with the current European [10], American [28] and Australian [29] design rules revealed generally conservative and scattered resistance predictions, while comparisons with the DSM-based design proposals developed by Dinis and Camotim [3] were more accurate but with some predictions on the unsafe side. New design proposals were subsequently made. Filipovic et al. investigated the behaviour and capacity of pin-ended hot-rolled [16] and laser-welded [17] stainless steel angles under compression through physical experiments and compared the results with the European [10] and Australian [29] resistance predictions, which were shown to be generally conservative. Dobric et al. conducted laboratory tests [20] as well as numerical simulations [24,25] on pin-ended cold-formed stainless steel angle section members under compression and also highlighted the high scatter in the resistance predictions of the European [10] and Australian [29] design standards. New flexural buckling curves were proposed by Dobric et al. for cold-formed [24,26] and laser-welded [25] angles on the basis of the test and FE results.

Pin-ended stainless steel angle section columns have been the focus of a number of recent studies, but the available test data remain rather scarce and, as far as the authors are aware, no tests have been reported on stainless steel angles under combined loading. Therefore, in the current study, tests are carried out on pin-ended hot-rolled stainless steel equal-leg angle section members under compression and combined loading, with bending allowed about the minor axis. Numerical models are then validated and subsequently used to generate additional results to underpin the development of improved design rules for these members.

For short-to-intermediate-length equal-leg angle section columns, torsional-flexural buckling is critical. Although torsional and major-axis flexural buckling modes always occur in combination in such members, the torsional mode has a significantly greater contribution for shorter angles. Since it was shown in [4,30] that torsional and local buckling are identical for equal-leg angle section columns (with the exception of cases where the outstand aspect ratio is less than one), the torsional portion of the aforementioned combined mode may be treated simply as local buckling and similar secondary effects also may be assumed to occur. When angle section members with slender legs are subjected to compression, local/torsional buckling causes the axial stresses to redistribute. This results in the centroid of the cross-section shifting away from the geometric centroid, as shown in Fig. 2; for equal-leg angles, this shift in effective centroid only occurs along the line of major u–u axis, owing to the symmetry of the cross-section about this axis. In concentrically-loaded pin-ended members, the shift in effective centroid creates an eccentricity $e_{\mathrm{N},v}$ (equal to the shift in effective centroid — see Fig. 2) between the lines of action (i.e. the loading) and resistance (i.e. the effective centroid), which induces a bending moment

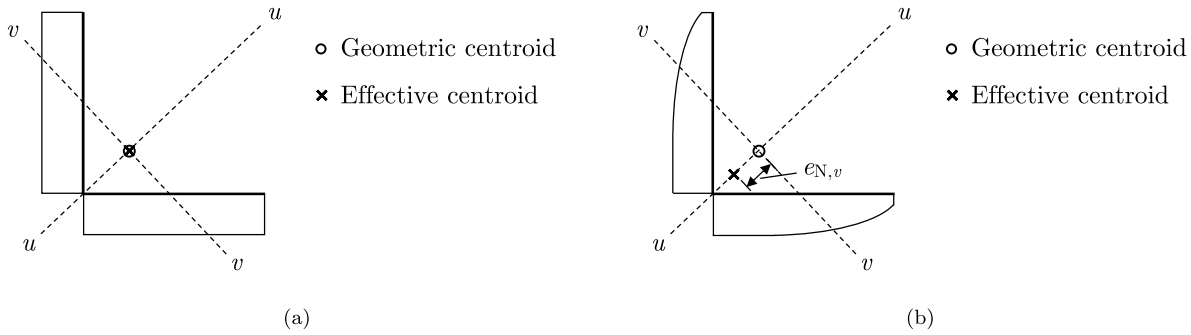

Fig. 2. Axial stress distribution and geometric and effective centroid position of equal-leg angle section under compression (a) prior to and (b) after local buckling.

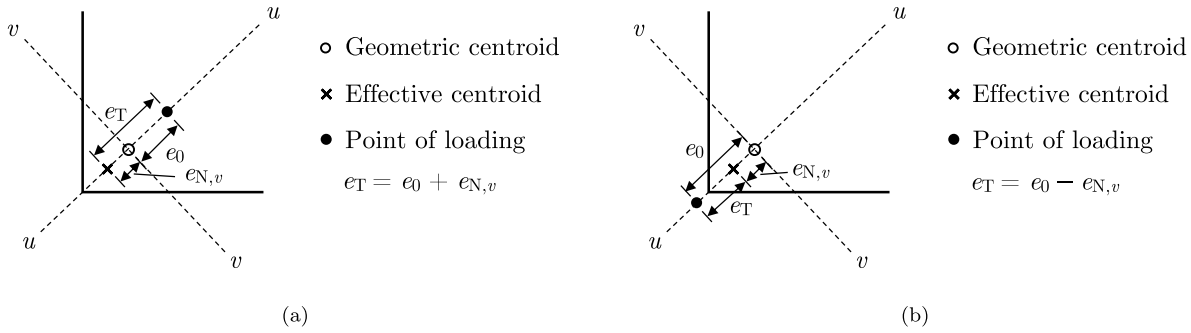

Fig. 3. Effect of the shift of effective centroid for cases where the point of loading (i.e. the initial applied loading eccentricity) is towards the (a) tips and (b) corner of the cross-section.

about the minor v–v axis. The column therefore becomes a beam–column, experiencing combined compression and bending. This effect does not impact upon fixed-ended angles since bending is restrained at the member ends.

For equal-leg angles that are initially eccentrically loaded with respect to the minor axis, depending on the direction of the initial eccentricity, the bending moments in the member may be either exacerbated (i.e. the shift in effective centroid further increases the eccentricity) or relieved (i.e. the shift in effective centroid reduces the eccentricity). Consequently, the resistance of the member will either be reduced or increased. The influence of the shift of the effective centroid on the total eccentricity e_T is presented in Fig. 3, where the shift of the effective centroid increases and reduces the total eccentricity when the point of loading (i.e. the initial applied loading eccentricity) is towards the tips (positive direction — see Fig. 3(a)) and the corner (negative direction — see Fig. 3(b)), respectively. Rasmussen [2] proposed an expression to predict the shift of the effective centroid in equal-leg angles, as given by:

$$e_{N,v} = \frac{5b}{16\sqrt{2}}\left(\frac{\bar{\lambda}_p - 1.22}{\bar{\lambda}_p - 0.22}\right). \quad (1)$$

This expression was developed based on the plate buckling curve given in the North American [31] and Australian [32] standards. By adopting the plate buckling curve for outstands in EN 1993-1-5 [33], the following, slightly modified expression, is obtained:

$$e_{N,v} = \frac{5b}{16\sqrt{2}}\left(\frac{\bar{\lambda}_p - 1.188}{\bar{\lambda}_p - 0.188}\right). \quad (2)$$

3. Experimental investigation

3.1. General

The experimental programme, the results of which are presented herein, involved material tensile coupon tests, initial geometric imperfection measurements and a total of 19 pin-ended stainless steel angle section buckling tests, comprising 5 column buckling tests and 14 tests on specimens subjected to combined compression and minor-axis bending. The tested cross-sections were hot-rolled equal-leg angles in Grade 1.4307 austenitic stainless steel; their cross-section geometries, alongside the respective chemical composition of the test materials, as reported in the manufacturer's mill certificate, are presented in Table 2.

3.2. Tensile coupon tests

Tensile coupon tests were conducted first to obtain the material properties of the studied stainless steel angle sections. Two coupons were extracted from the middle portion of both legs in the longitudinal direction (see Fig. 4) following the dimensional requirements specified in EN ISO 6892 [34]. The tensile tests were conducted using an Instron 250 kN testing machine. The strains in the longitudinal direction were recorded using two linear electrical resistance strain gauges that were attached to the centre of the front and back faces of the coupons at mid-height. A clip gauge with a gauge length of 100 mm was placed within the parallel length; the extension was recorded and used to obtain the average strain over the gauge length. The tensile test set-up is shown in Fig. 5. The engineering stress–strain curves from the tensile coupon tests are presented in Fig. 6. The first stage of the stress–strain curves, up to the strain value of 10%, was obtained using the strain gauge readings, while the second stage of the curves until fracture was derived based on the clip gauge readings. The obtained average mechanical

Table 2
Chemical composition of tested cross-sections from mill certificate.

Cross-section	C (%)	P (%)	S (%)	Si (%)	Mn (%)	Cr (%)	Ni (%)	Mo (%)
80 × 80 × 6	0.016	0.031	0.001	0.342	1.515	18.105	8.035	0.268
100 × 100 × 12	0.023	0.031	0.001	0.355	1.470	18.075	8.070	0.246
100 × 100 × 10	0.025	0.032	0.002	0.413	1.500	18.285	8.045	0.331

Table 3
Average measured material properties of the tested cross-sections from tensile coupon tests.

Cross-section	E (N/mm^2)	f_y (N/mm^2)	$f_{1.0}$ (N/mm^2)	f_u (N/mm^2)	ϵ_u (%)	ϵ_f (%)	n	m_u	$m_{1.0}$
80 × 80 × 6	214 200	336	410	742	59.2	61.7	13.5	3.9	3.1
100 × 100 × 12	188 600	307	356	665	52.3	53.9	10.9	3.1	2.2
100 × 100 × 10	206 300	324	372	671	46.8	48.2	18.1	3.2	2.4

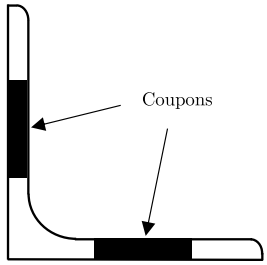

Fig. 4. Location of tensile coupons within the angle section.

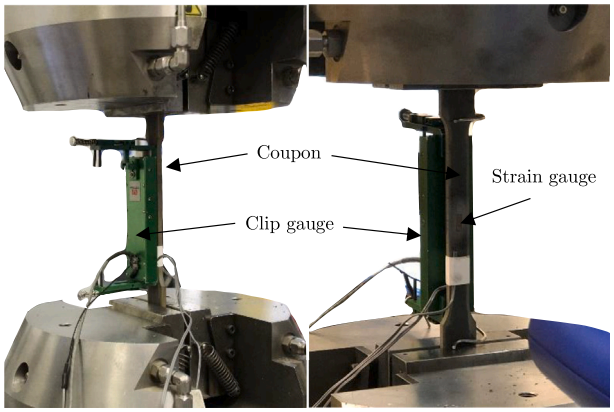

Fig. 5. Tensile coupon test set-up.

properties are presented in Table 3, where E is the Young's modulus, f_y and $f_{1.0}$ are the 0.2% and 1.0% proof stresses, respectively, ϵ_u is the strain at the ultimate stress f_u, ϵ_f is the fracture strain measured over the 100 mm gauge length, while n, m_u and $m_{1.0}$ are the Ramberg–Osgood strain hardening exponents, with m_u and $m_{1.0}$ corresponding to the models described in [35–39], respectively.

3.3. Initial geometric imperfection measurements

Initial geometric imperfections in the angle section specimens, including the bow imperfections about the minor and major axes, denoted as $\delta_{0,v}$ and $\delta_{0,u}$, respectively, and the twist ϑ along the member length, were measured prior to testing. The three modes of imperfection are presented in Fig. 7. The global bow and twist imperfections were determined using the same imperfection rig as employed in previous studies [5–7,40]. The set-up and approach for measuring and calculating the initial imperfections were presented in detail in [5]. Typical measured longitudinal distributions of initial global and torsional geometric imperfections are presented in Fig. 8, where local imperfections

Table 4
Summary of initial geometric imperfection amplitude measurements.

Buckling test	ID	$L/\delta_{0,v}$	$L/\delta_{0,u}$	ϑ/L (deg/m)
Column	1	2273	2500	0.14
	2	1217	2000	0.10
	3	4130	1267	0.19
	4	4706	1714	0.18
	5	2900	1000	0.72
	6	2857	1026	0.15
Beam–column	7	1429	870	0.15
	8	952	2660	0.20
	9	1000	1735	0.14
	10	1739	1379	0.06
	11	1379	3980	0.12
	12	2000	5714	0.10
	13	2373	5596	0.07
	14	7000	2800	0.06
	15	3182	2642	0.02
	16	1944	3111	0.01
	17	2295	2979	0.01
	18	7368	4239	0.05
	19	5833	3585	0.01
	Mean	2978	2673	0.13
	CoV	0.66	0.54	1.19

of very low amplitude can also be observed. A half-sine wave was employed to represent the shape of the imperfections, with the amplitude being taken as the maximum measured deviation from straightness. A summary of the measured initial geometric imperfection amplitudes of the specimens relative to the member length L is provided in Table 4.

3.4. Member buckling tests

Tests on 19 hot-rolled Grade 1.4307 austenitic stainless steel equal-leg angle section members - 5 columns and 14 beam–columns - were performed to study their buckling response and load-carrying capacity. The members were cylindrically pinned about the minor axis. For the column tests, the member lengths L were varied to cover a range of member slenderness $\bar{\lambda}$ values, where minor-axis flexural buckling was critical for all members. Two member lengths were chosen for the beam–column tests; torsional-flexural buckling was critical for the shorter members and minor-axis flexural buckling was critical for the longer members. The initial loading eccentricities were varied in size and direction to study the ultimate strength of stainless steel equal-leg angles subjected to a range of combinations of axial compression and bending.

The buckling tests were conducted using an Instron 2000 kN hydraulic testing machine under displacement control. Knife edges were used at both ends of the members to allow rotation about the minor axis and prevent rotation about the longitudinal and major axes, which created cylindrically pin-ended boundary conditions. End plates were welded to both ends of each specimen, which were inserted into special clamps connected to the knife edges. The specimens were then

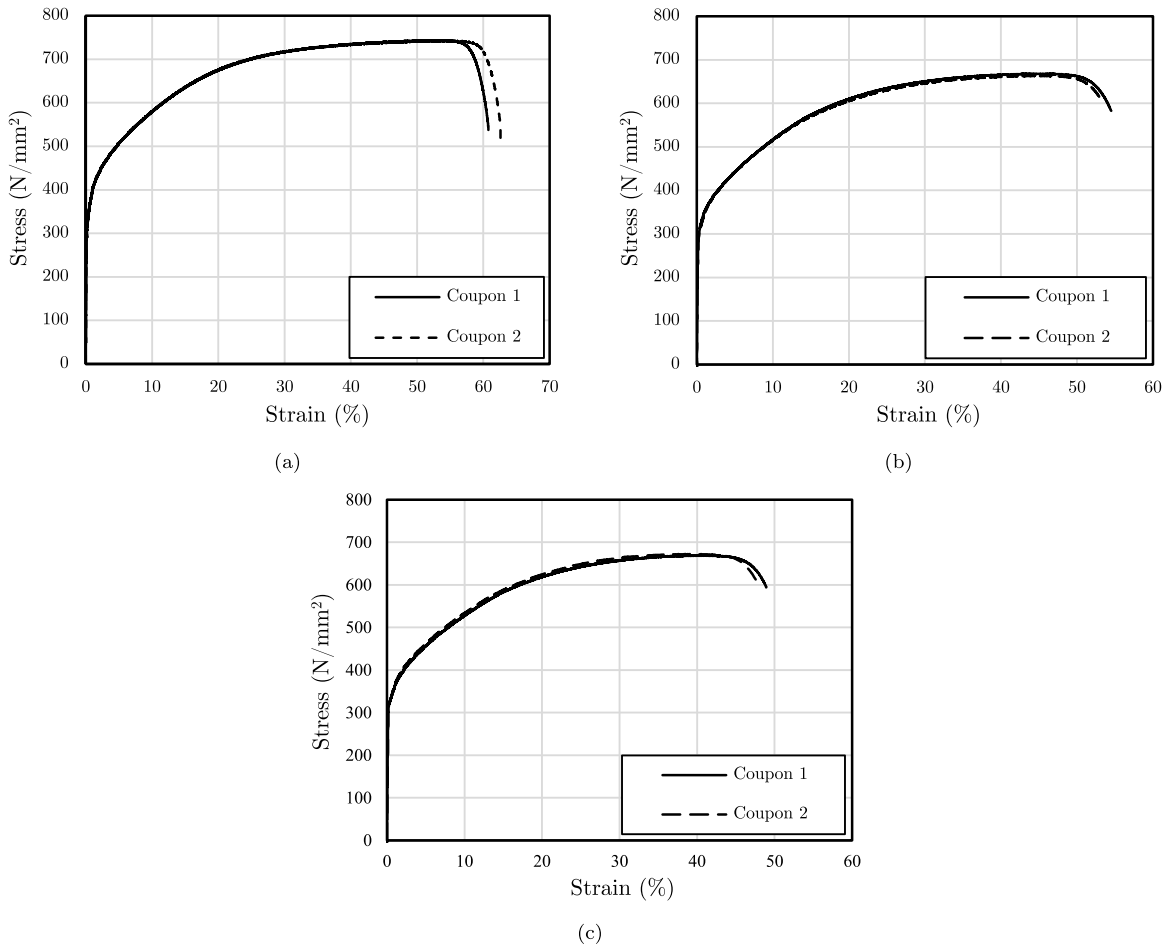

Fig. 6. Measured engineering stress–strain curves from tensile coupon tests for (a) 80 × 80 × 6, (b) 100 × 100 × 12 and (b) 100 × 100 × 10 angle sections.

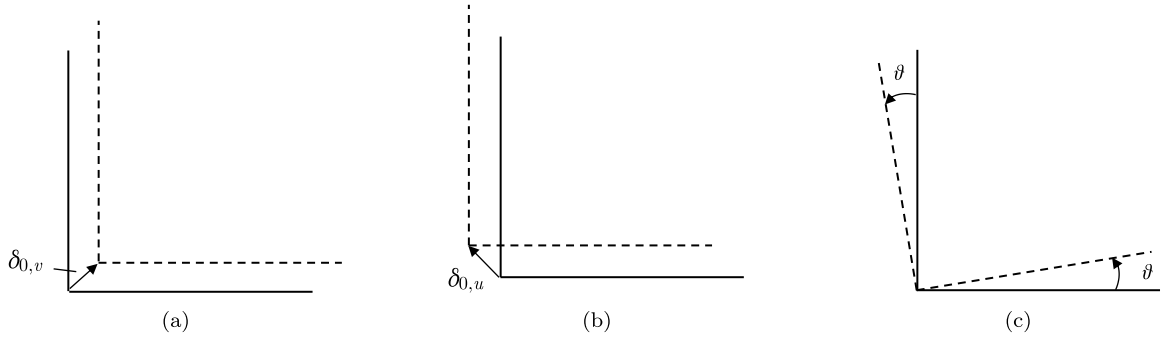

Fig. 7. Illustrations of amplitudes of imperfection shapes for (a) minor-axis flexural, (b) major-axis flexural and (c) torsional modes.

adjusted to achieve the required initial loading eccentricity, before the tightening of bolts on the clamp. Two LVDTs were used to measure the end-shortening and minor-axis lateral deflection of the specimens at mid-height. Four string pots, attached to the corner and the tips of both legs of the angle section members, were employed to measure the twist at mid-height. Six electrical resistance strain gauges were affixed to the specimens at mid-height to measure the longitudinal strains at the corner and the tips of the angles. Two inclinometers were used to measure rotations at the member ends. The configuration of the string pots and strain gauges is shown in Fig. 9 and the test set-up is presented in Fig. 10. The key test results, including the load, machine displacement and readings from the strain gauges, LVDTs, string pots and inclinometers were recorded at 0.5 s intervals using the data acquisition equipment DATASCAN and logged using the DSLOG software. A global imperfection amplitude of $L/1000$ is typically assumed in the development of column buckling design provisions [41–43]. Therefore, for the column buckling tests, a total global imperfection amplitude ω_g about the minor axis, defined as the sum of the initial bow imperfection $\delta_{0,v}$ and the initial loading eccentricity $e_{0,v}$, was set to $L/1000$ by adjusting the initial loading eccentricity. This was achieved by preloading the specimens up to 20% of the predicted ultimate load and back calculating the total global imperfection ω_g using Eq. (3), where I is the second moment of area about the axis of buckling (i.e. the minor axis), ϵ_{max} and ϵ_{min} are the average strains recorded by the strain gauges on the concave and convex sides of the specimens, respectively, N is the applied axial load, H is the distance between the strain gauges and δ is the measured lateral deflection at the mid-height.

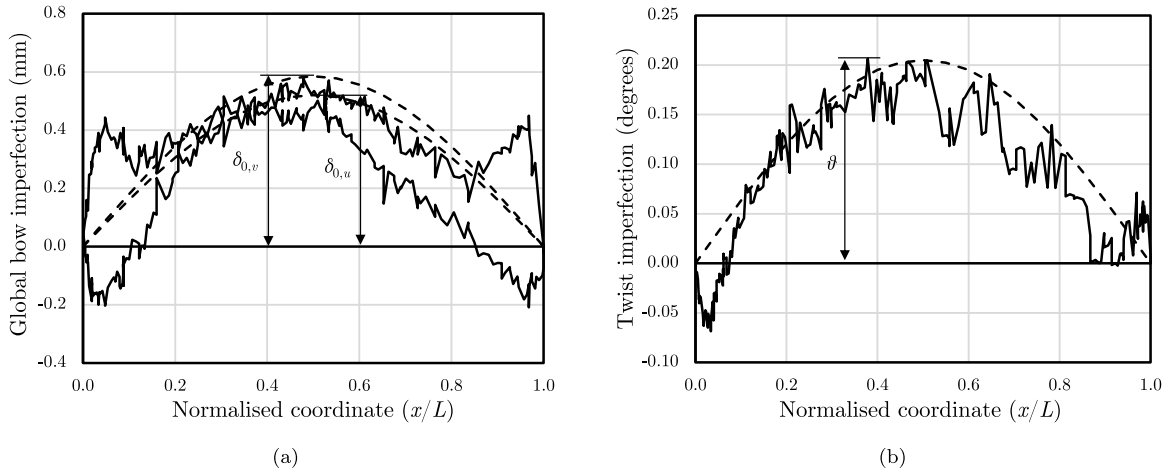

Fig. 8. Typical measured initial (a) global bow and (b) twist geometric imperfections versus normalised position along the member length (x/L), with dashed lines marking representative half-sine waves.

The initial loading eccentricity was then adjusted and the procedure repeated until ω_g reached a value close to $L/1000$, though in many cases, the achieved values deviated somewhat from this target.

$$\omega_g = \frac{EI(\epsilon_{max} - \epsilon_{min})}{HN} - \delta. \quad (3)$$

For the beam–column test specimens, the initial loading eccentricities were back calculated after the experiments using a similar procedure. Positive and negative ω_g values imply that the initial loading eccentricity was applied towards and away from the tips of the cross-section legs, respectively. A typical plot of load N against ω_g/L, shown for Specimen 11, is presented in Fig. 11, where the initial eccentricity ω_g = 36.7 mm was determined. The geometry and notation of the test specimens are presented in Fig. 12, while a summary of the measured geometric properties of the test specimens and the key results from the column and beam–column buckling tests are presented in Tables 5 and 6, respectively. Graphs of the test axial load versus (a) end-shortening and (b) mid-height lateral deflection about the minor axis are plotted in Fig. 13 for the columns and Figs. 14 and 15 for the beam–columns. All tested specimens failed by minor-axis flexural buckling, and the direction of buckling was dictated by the direction of the minor-axis initial global imperfection for the columns and the loading eccentricity for the beam–columns (see Fig. 16). A comparison of the column buckling test data with the flexural buckling curve (with limiting slenderness $\bar{\lambda}_0 = 0.2$ and imperfection factor $\alpha = 0.76$) for angle section members set out in prEN 1993-1-4 [44] is presented in Fig. 17(a), where $\chi = N_u/Af_y$ is the buckling reduction factor with N_u being the ultimate load reached during the test. Note that the predicted shift of effective centroid is zero for the presented test specimens, allowing direct comparisons to be made between the experimental results and the column buckling curve. Comparisons of the beam–column test data with the N–M interaction curve for I-sections set out in prEN 1993-1-4 [44] are presented in Figs. 17(b) and 17(c) for the specimens with L = 400 mm and L = 1400 mm, respectively, where the ultimate load N_u and moment M_u are normalised against the compression $N_{b,prop}$ and bending moment $M_{b,prop}$ resistances proposed in [4,7]. Both the column and beam–column test results generally follow the trend of the buckling curve and N–M interaction curves, respectively, and lie consistently on the safe side.

4. Numerical modelling

The commercial finite element (FE) software ABAQUS was used herein to create numerical models to simulate the mechanical behaviour of pin-ended stainless steel equal-leg angle section members under compression and combined compression and bending. The FE models are first validated in Section 4.2 by comparing the results against the existing and newly generated experimental data on pin-ended stainless steel equal-leg angles. In Section 4.3, a parametric study is presented to investigate the behaviour of both hot-rolled and cold-formed stainless steel equal-leg angle section members free to rotate about the minor axis and subjected to compression and combined loading; a range of cross-section geometries, member lengths and load combinations are studied.

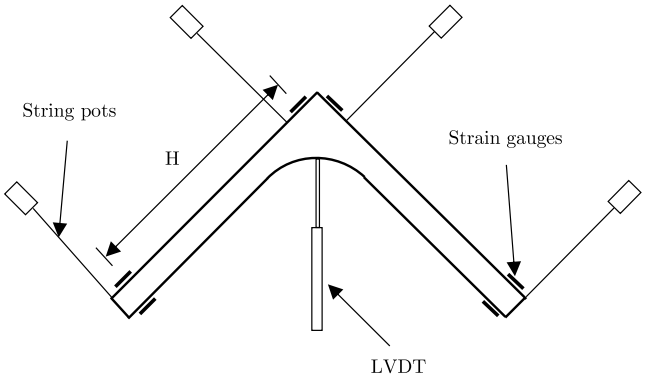

Fig. 9. Configuration of strain gauges, string pots and LVDT at the mid-height of the column specimens.

4.1. General modelling assumptions

Similar modelling assumptions to those used in [4–7] were adopted, which are briefly described herein. The 4-noded shell element, S4R [45], with reduced integration, 6 degrees of freedom (3 translational and 3 rotational) at each node and hourglass control, was employed to model the angle section members; this element type has been successfully utilised in similar previous studies [46–48]. A mesh size of approximately 5 mm, typically resulting in at least 10 elements across each leg of the angles, was utilised.

Both hot-rolled and cold-formed stainless steel angles were modelled. For the hot-rolled angles, the root fillet was modelled by introducing thicker elements at the junction between the angle section legs and the thickness was offset to avoid overlapping of the two legs, which were connected using BEAM-type multi-point constraints (MPC), as shown in Fig. 18(a). The rounded corner of the cold-formed angles was represented by employing a finer mesh in the curved corner region than in the flat regions, as shown in Fig. 18(b). To model the load

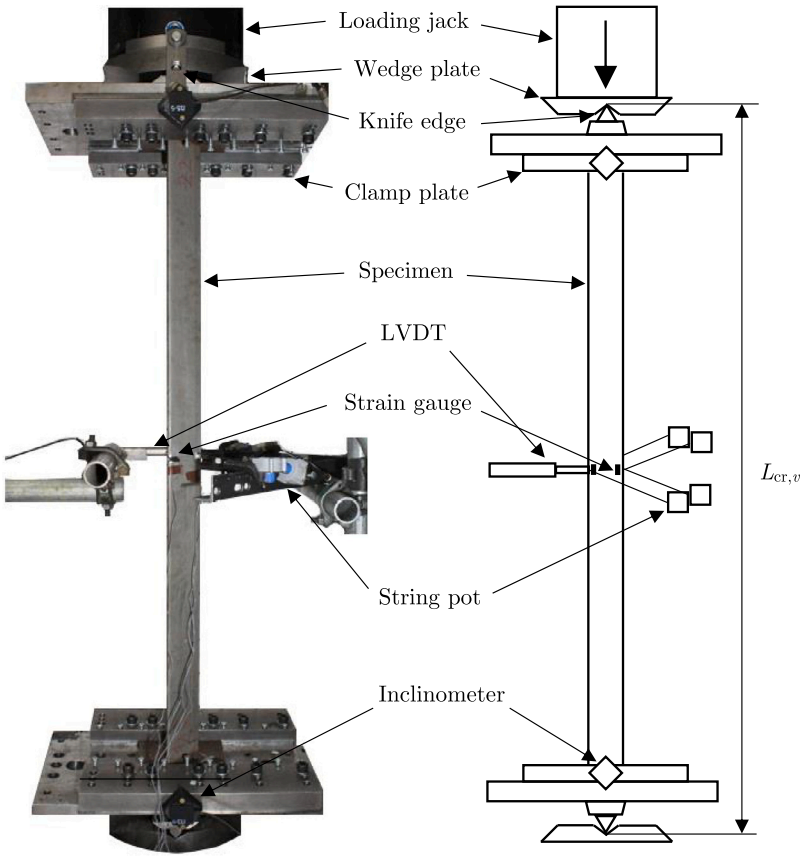

Fig. 10. Photographic and schematic representation of column and beam–column buckling test set-up.

Table 5
Summary of measurements of geometric properties, initial loading eccentricities and ultimate loads for column buckling test specimens.

Cross-section	ID	b (mm)	t (mm)	r_1 (mm)	r_2 (mm)	L (mm)	$L_{cr,v}$ (mm)	$\bar{\lambda}$	ω_g (mm)	N_u (kN)
80 × 80 × 6	1	80.08	6.50	7.0	3.5	1000	1150	0.90	1.00	214.93
	2	80.18	6.46	7.0	3.5	1398	1548	1.22	3.75	137.30
	3	80.18	6.45	7.0	3.5	1901	2051	1.61	3.00	92.48
	4	80.23	6.45	7.0	3.5	2398	2548	2.00	3.70	59.86
	5	80.21	6.46	7.0	3.5	2897	3047	2.35	6.10	42.99

Table 6
Summary of measurements of geometric properties, initial loading eccentricities and ultimate loads for beam–column buckling test specimens.

Cross-section	ID	b (mm)	t (mm)	r_1 (mm)	r_2 (mm)	L (mm)	$L_{cr,v}$ (mm)	$\bar{\lambda}_{TF}$ or $\bar{\lambda}$	ω_g (mm)	N_u (kN)
100 × 100 × 12	6	100.75	11.95	10.0	5.0	400	550	0.42	−23.80	349.85
	7	100.78	12.00	10.0	5.0	400	550	0.42	−5.50	594.82
	8	100.78	11.99	10.0	5.0	399	549	0.42	0.10	740.72
	9	100.92	11.98	10.0	5.0	399	549	0.42	0.55	741.84
	10	100.73	11.99	10.0	5.0	400	550	0.42	7.40	552.64
	11	100.70	12.01	10.0	5.0	398	548	0.42	36.70	266.03
	12	100.64	12.00	10.0	5.0	400	550	0.42	146.00	87.94
100 × 100 × 10	13	100.00	9.86	10.0	5.0	1399	1549	0.97	−28.90	160.87
	14	100.04	9.85	10.0	5.0	1400	1550	0.97	−10.70	254.82
	15	100.05	9.84	10.0	5.0	1400	1550	0.97	−1.60	401.77
	16	100.08	9.86	10.0	5.0	1400	1550	0.97	4.80	314.16
	17	99.95	9.91	10.0	5.0	1400	1550	0.98	20.60	206.41
	18	99.86	9.84	10.0	5.0	1399	1549	0.98	46.50	132.76
	19	99.89	9.82	10.0	5.0	1398	1548	0.97	138.00	63.51

applied to the members, a longitudinal displacement was imposed at one end through a reference point that was free to move longitudinally. The geometrically and materially nonlinear analyses were executed using the Riks arc-length method [49]. To validate the FE models, experiments reported in the literature, as well as those conducted in the current study, were simulated. The measured geometric properties and stress–strain curves were employed in these analyses. Throughout the parametric study, the two-stage Ramberg–Osgood material model [35–38], with typical values [50] for the key mechanical properties, was utilised. A Poisson's ratio of 0.3 in the elastic range was assumed in all cases. The material properties were input into ABAQUS in the form of true stress σ_{true} and true plastic strain ϵ_{true}, converted from

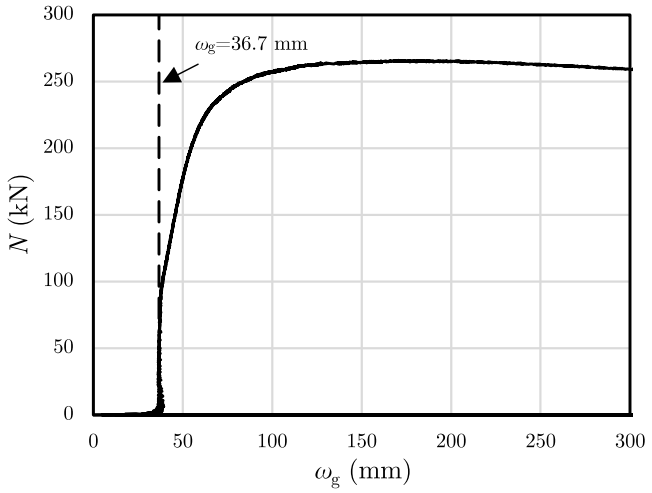

Fig. 11. Typical plot of load N against ω_g for Specimen 11, where the initial eccentricity ω_g = 36.7 mm.

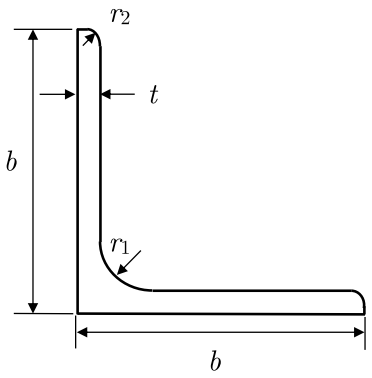

Fig. 12. Geometry and notation for equal-leg angle sections.

the measured engineering stress σ and strain ϵ using the well-known relationships:

$$\sigma_{\text{true}} = \sigma\,(1+\epsilon)\,, \tag{4}$$

$$\epsilon_{\text{true}} = \ln(1+\epsilon) - \frac{\sigma_{\text{true}}}{E}. \tag{5}$$

For the hot-rolled stainless steel angles, a bilinear residual stress distribution with a peak value of 70 MPa, constant with thickness and leg width, was employed [4–7], as illustrated in Fig. 19, where the negative sign indicates compressive stress and the positive sign denotes tensile stress. The residual stresses were input into ABAQUS using the *INITIAL CONDITIONS command. For the cold-formed stainless steel angles, the dominant bending residual stresses were assumed to be inherently captured in the material stress–strain curves [51,52], with a lower value for the strain hardening exponent n than for hot-rolled material, and were therefore not explicitly defined. For the validation study, the measured initial major-axis global bow and twist imperfection amplitudes, as presented in Table 4, were applied; about the minor axis, the measured loading eccentricity values given in Tables 5 and 6, which included the minor-axis global bow imperfections, were employed. However, where measured data were not available, and throughout the parametric study, a half-sine wave function over the member length with an amplitude of $L/1000$ at mid-span was adopted about both principal axes for the initial bow imperfections. The direction of the minor-axis bow imperfection was chosen to provide the lowest resistance in the parametric study, which was towards the corner of the section for the pin-ended columns and in the same direction as bending

Table 7
Summary of comparisons of FE model ultimate loads $N_{\text{u,FE}}$ with those obtained experimentally $N_{\text{u,Test}}$.

Source	No. of tests	$\frac{N_{\text{u,FE}}}{N_{\text{u,Test}}}$			
		Mean	CoV	Min	Max
Zhang et al. [22]	12	0.98	0.06	0.91	1.09
Zhang et al. [23]	12	0.98	0.04	0.93	1.03
Present study	19	0.99	0.04	0.90	1.06
Total	43	0.98	0.04	0.90	1.09

(i.e. in the opposite direction to the initial eccentricity) for the beam–columns. A similar shape was also adopted for the initial twist with an amplitude of $\vartheta = \arctan(L/1000b)$ at mid-span. Boundary conditions were applied to the supports through kinematic coupling constraints to link all the degrees of freedom (translational and rotational) of the member end-nodes to two reference points. Cylindrically pin-ended boundary conditions were created by restraining the necessary degrees of freedom at the reference points, where longitudinal displacement (i.e. end-shortening) and rotation about the axis of bending (i.e. the minor axis) were free and the remaining degrees of freedom were fixed; warping was also prevented at both ends.

4.2. Validation

The FE models were validated against the 19 tests from the present study together with a total of 24 existing experiments on pin-ended stainless steel angle section columns; a summary of the comparisons between the ultimate loads from the FE models and those obtained experimentally is presented in Table 7 and Fig. 20. Overall, there is good agreement between the test and FE ultimate loads, with a mean $N_{\text{u,FE}}/N_{\text{u,Test}}$ ratio (where $N_{\text{u,FE}}$ and $N_{\text{u,Test}}$ are the ultimate loads from the FE models and tests, respectively) of 0.98 and a coefficient of variation (CoV) of 0.04. In addition to the FE model validation presented herein, the developed FE model has also been demonstrated to be suitable for simulating the structural response of equal-leg angle section members with different material characteristics under various loading conditions in several recent studies [4–7]. Comparisons of typical load–deformation curves, shown for Specimen 11 tested in the current study, are presented in Fig. 21, illustrating good agreement between the test and FE results. Note that the slightly lower initial stiffnesses obtained from the experiments relative to the FE models are attributed to the use of the machine displacement to determine the end shortening of the test specimens, which includes some additional flexibility in the test rig. The described comparisons demonstrate the ability of the developed FE models to predict the physical behaviour observed in experiments on pin-ended stainless steel angle section columns and beam–columns, and confirm their suitability for performing a parametric study.

4.3. Parametric study

Following validation of the numerical models, a parametric study was conducted, as presented currently. The FE models were used to generate additional data for hot-rolled and cold-formed pin-ended angle section columns and beam–columns in the three main families of stainless steel (i.e. austenitic, duplex and ferritic), considering a wide range of cross-section geometries, member lengths and load combinations. A summary of the material properties adopted in the parametric study, taken from [50], is presented in [5]. Leg widths b of 50 mm and 100 mm were analysed, while the thicknesses t and member lengths L were varied to evaluate a spectrum of normalised slendernesses, $\bar{\lambda}_{\text{TF}}$ or $\bar{\lambda}$, and elastic buckling load $N_{\text{cr,TF}}/N_{\text{cr,F},v}$ ratios. The b/t ratios ranged between 8 and 50, while the L/b ratios ranged between 1 and 100 (see Table 8). In addition, the initial eccentricities were varied both in direction (towards and away from the corner of the angles)

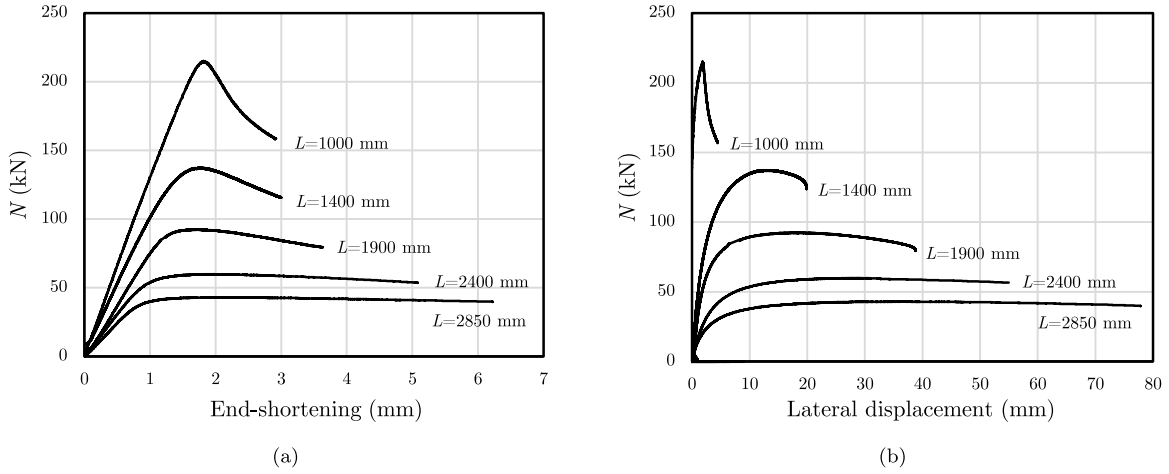

Fig. 13. Axial load N versus (a) end-shortening and (b) mid-height minor-axis lateral deflection for the pin-ended column test specimens, the nominal lengths L of which are indicated on the figure.

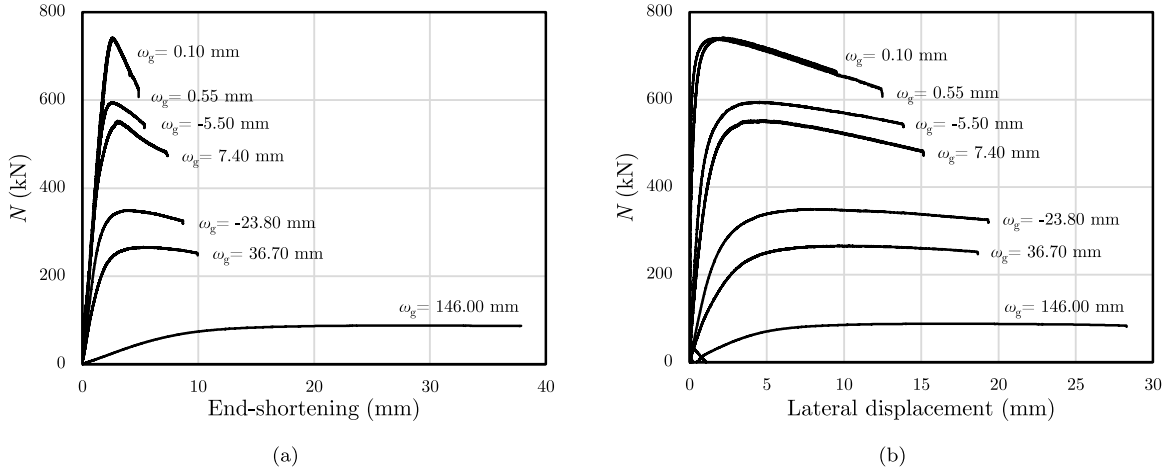

Fig. 14. Axial load N versus (a) end-shortening and (b) mid-height minor-axis lateral deflection for the pin-ended beam–column test specimens with L = 400 mm, the eccentricities ω_g of which are indicated on the figure.

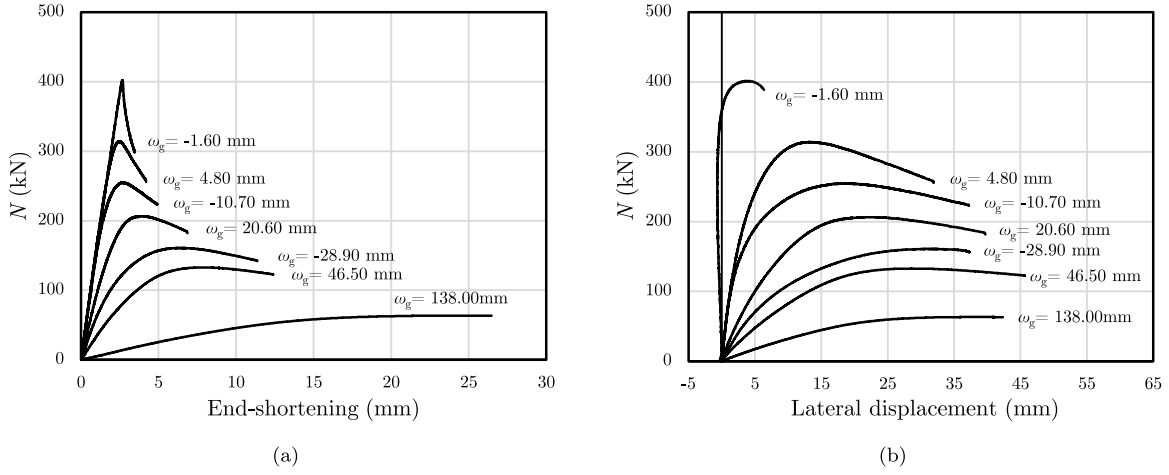

Fig. 15. Axial load N versus (a) end-shortening and (b) mid-height minor-axis lateral deflection for the pin-ended beam–column test specimens with L = 1400 mm, the eccentricities ω_g of which are indicated on the figure.

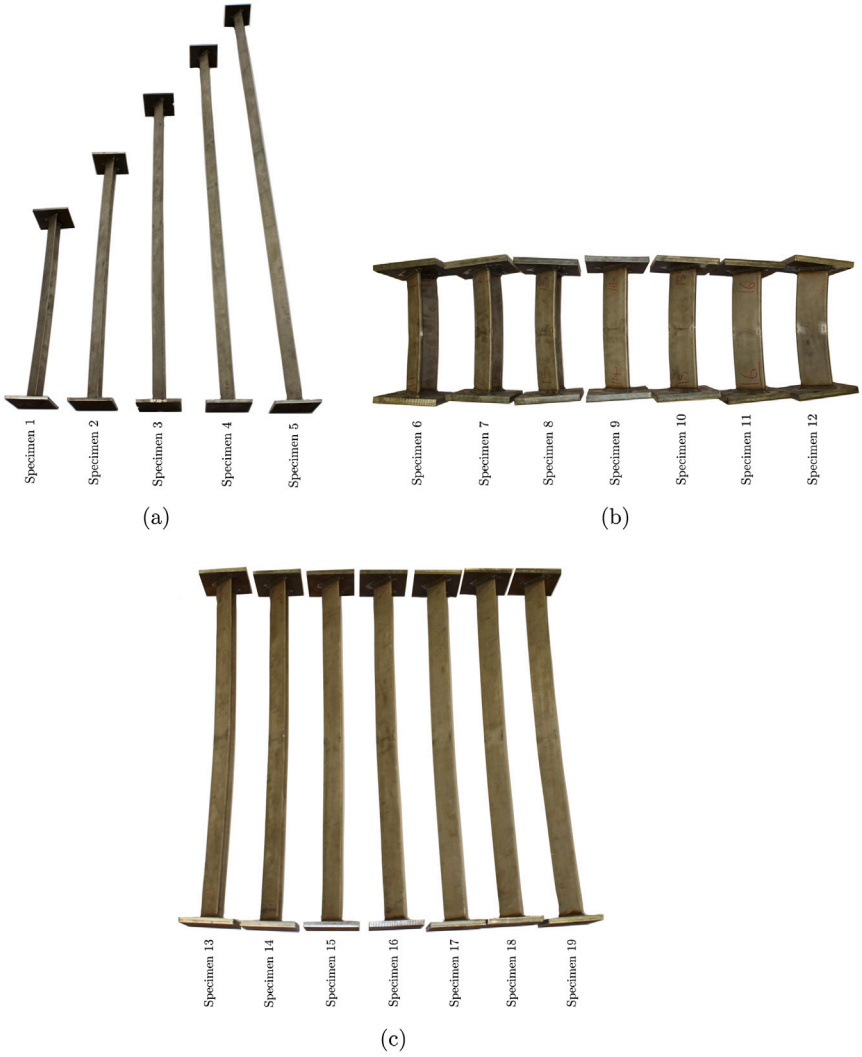

Fig. 16. Presentation of deformed specimens tested under (a) compression, (b) combined loading with $L = 400$ mm and (c) combined loading with $L = 1400$ mm.

and magnitude to study a wide range of load combinations. In total, 7920 FE results (120 with zero eccentricity, 600 with positive and 600 with negative eccentricities for 6 production type and stainless steel family combinations) were generated. The results are presented in Figs. 22(a) and 22(b) for positive and negative loading eccentricities, respectively, in which the normalised axial load $N_u/N_{b,prop}$ (where N_u is the ultimate load obtained from the tests or FE models and $N_{b,prop}$ is the axial compression resistance of the members, determined as described in [5]) is plotted against the corresponding normalised bending moment $M_u/M_{b,prop}$ (where $M_u = N_u e_T$ is the ultimate bending moment obtained from the tests or FE models and $M_{b,prop}$ is the bending resistance of the members, determined as described in [7]). The results for the angles where the eccentricities were applied in the positive direction (i.e. the tips of the cross-section legs are in compression) are shown in Fig. 22(a), while the results for the cases where the eccentricities were applied in the negative direction (i.e. the tips of the cross-section legs are in tension) are shown in Fig. 22(b). For reference, the interaction curve from prEN 1993-1-4 [44] for I-section members (since there is no guidance for angle section members) with $\bar{\lambda} = 3.0$ is also shown in the figures. Note that, to account for the additional bending moment caused by the shift of effective centroid, the expression proposed by Rasmussen [2], as presented in Section 2, is adopted.

Table 8
Summary of ranges of key varied parameters in FE parametric study.

Compression side	b/t	L/b	$N_{cr,TF}/N_{cr,F,v}$	$\bar{\lambda}_{TF}$ or $\bar{\lambda}$
Section tips	8–50	1–100	0.05–14.00	0.2–5.0
Section corner	8–50	1–100	0.05–14.00	0.2–5.0

5. Analysis and discussion of results

As can be seen in Fig. 22, depending on the direction of the initial loading eccentricity, the behaviour and resistance of pin-ended equal-leg angle section beam–columns may vary. This was further investigated by studying the behaviour and resistance of pin-ended equal-leg angle section members with different local slendernesses ($\bar{\lambda}_p = 1.0$ and $\bar{\lambda}_p = 2.0$) subjected to different initial global bow imperfection directions (where $\delta_0 > 0$ and $\delta_0 < 0$ are global bow imperfections towards and away from the cross-section tips, respectively) and a spectrum of loading eccentricities. The normalised ultimate resistance N_u/N_{cr} (where N_u is the peak load and N_{cr} is the lowest elastic critical buckling load) is plotted against the initial applied loading eccentricity e_0 in Figs. 23(a) and 23(b) for angles with $\bar{\lambda}_p = 1.0$ and $\bar{\lambda}_p = 2.0$, respectively. The corresponding equilibrium paths are presented in Figs. 24(a) and 24(b), respectively, where the normalised load N/N_{cr} is plotted against the sum of the initially applied loading eccentricity e_0 and the mid-height lateral deflection about the minor axis δ. As can bee

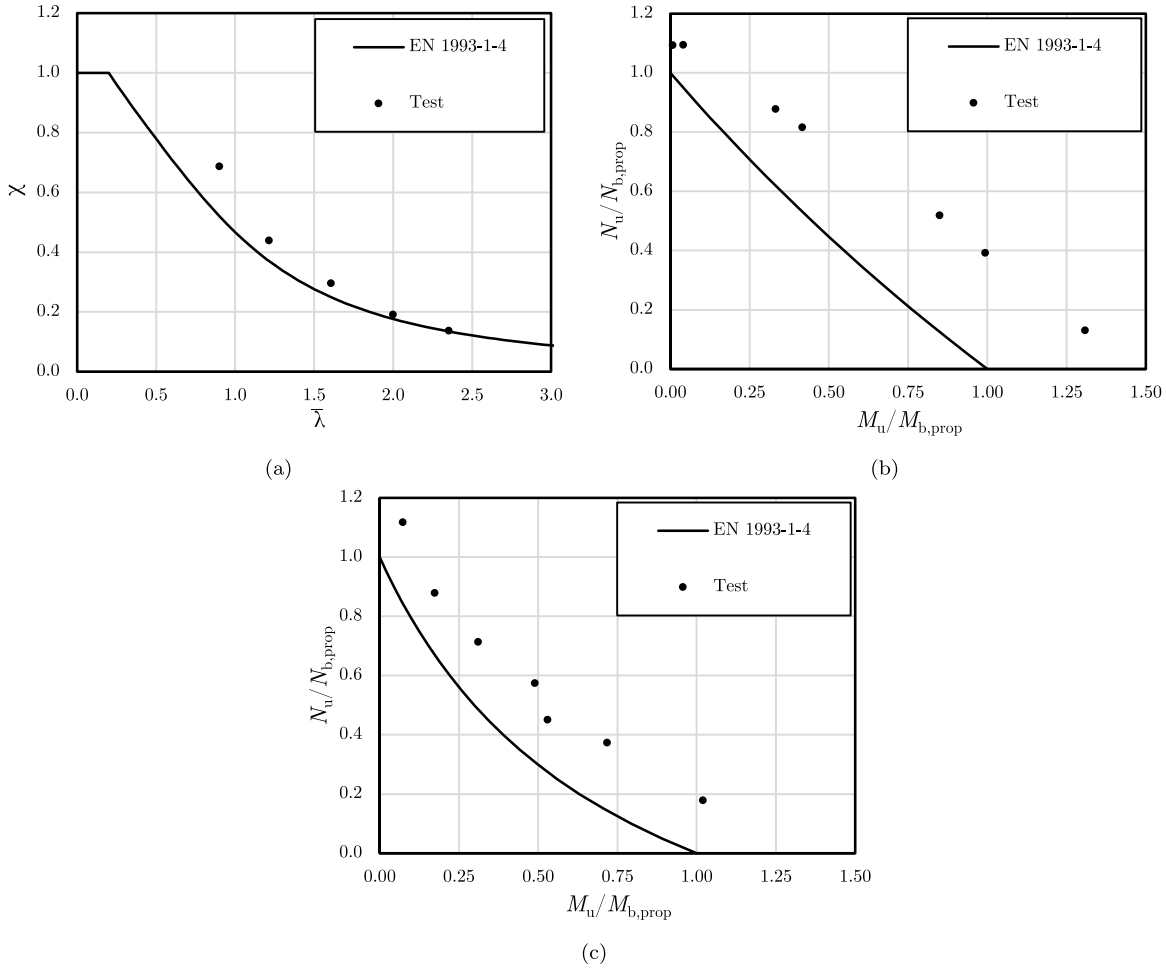

Fig. 17. Comparison of test data with (a) buckling curve for pin-ended column tests, (b) N–M interaction curve for beam–column test specimens with $L = 400$ mm and (c) N–M interaction curve for beam–column test specimens with $L = 1400$ mm.

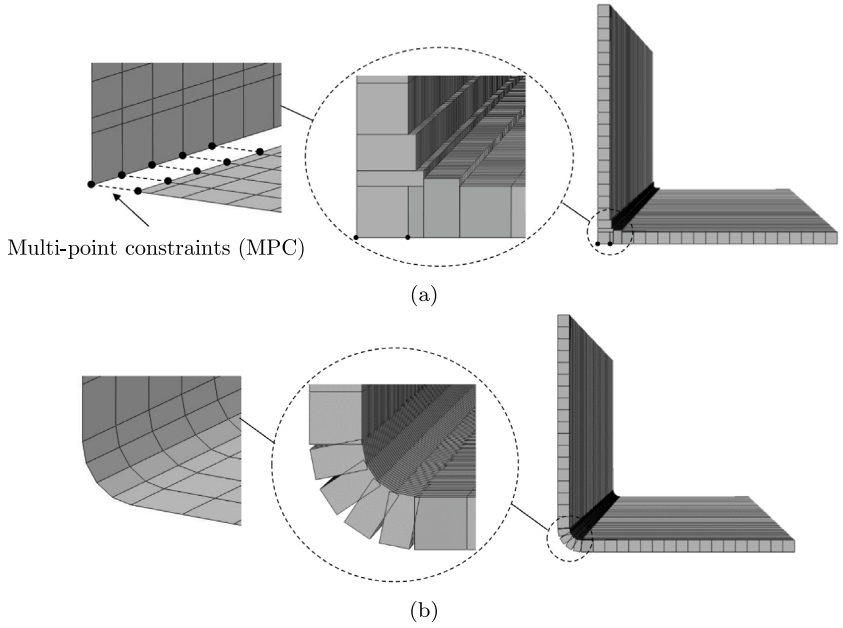

Fig. 18. FE representation of corner region in (a) hot-rolled and (b) cold-formed angle section members. Further details are provided in [5].

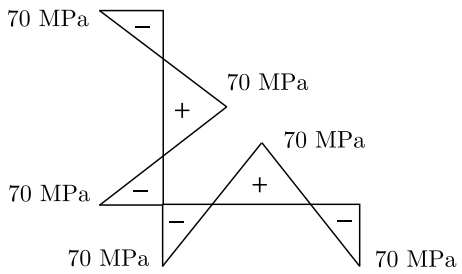

Fig. 19. Residual stress distribution employed for hot-rolled steel equal-leg angles in the present FE models.

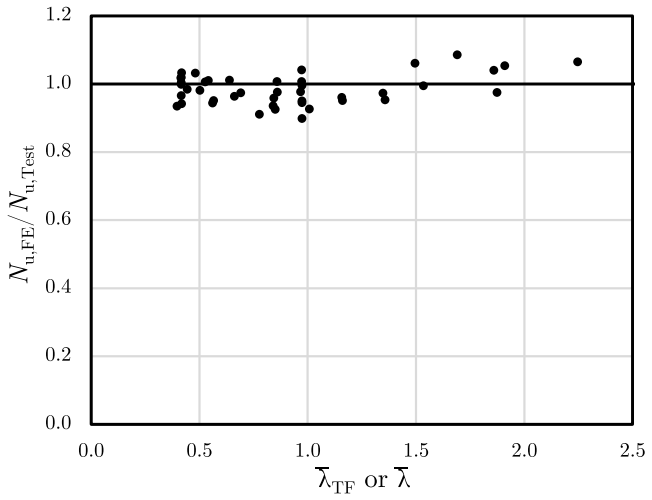

Fig. 20. Variation of ratios of FE model ultimate loads $N_{u,FE}$ to experimental ultimate loads $N_{u,Test}$ with normalised slenderness $\bar{\lambda}_{TF}$ or $\bar{\lambda}$, whichever is higher (i.e. critical).

seen, for the angles with $\bar{\lambda}_p = 1.0$, the ultimate resistances are similar for angles with the same eccentricity magnitude (i.e. the response is largely symmetric). However, for the angles with $\bar{\lambda}_p = 2.0$, there is a significant difference in equilibrium paths and ultimate resistances with eccentricity direction due to the shift of the effective centroid. For the angles with negative loading eccentricities (i.e. loading eccentricity applied towards the cross-section corner), the member benefits from the shift of the effective centroid and the ultimate resistance is enhanced, whereas for positive loading eccentricities (i.e. loading eccentricity applied towards the cross-section tips), the shift of the effective centroid reduces the resistance of the member under compression. This results in the asymmetric trend observed in Fig. 23(b). These findings are in line with Eq. (2), where the predicted shift of effective centroid is 0 and 1.0 mm for the studied angles with $\bar{\lambda}_p = 1.0$ and $\bar{\lambda}_p = 2.0$, respectively. It is worth mentioning that the aforementioned effects become negligible for very large loading eccentricities, since the shift in effective centroid is dwarfed by the applied loading eccentricity (i.e. $e_0 \gg e_{N,v}$).

6. Design of pin-ended stainless steel angle section columns and beam–columns to Eurocode 3

According to prEN 1993-1-4 [44], members subjected to combined loading with bending about the minor v–v axis and axial compression should satisfy the following criterion:

$$\frac{N_{Ed}}{\left(\frac{\chi_v N_{Rk}}{\gamma_{M1}}\right)} + k_{vv}\frac{\left(M_{v,Ed} + \Delta M_{v,Ed}\right)}{\left(\frac{M_{v,Rk}}{\gamma_{M1}}\right)} \leqslant 1.0. \tag{6}$$

Here, N_{Ed} and $M_{v,Ed}$ are the design values of the compression force and maximum bending moment about the minor v–v axis along the member length, respectively, and N_{Rk} and $M_{v,Rk}$ are the characteristic values of the cross-sectional resistance to compressive axial force and bending moment about the minor v–v axis, respectively. The quantity $\Delta M_{v,Ed}$ is the bending moment that arises due to the shift of the effective centroid about the minor v–v axis, $e_{N,v}$, for Class 4 cross-sections, which is based on the effective width b_{eff} [33] and given for equal angles thus:

$$e_{N,v} = \frac{b_{eff}}{\sqrt{2}}. \tag{7}$$

The term χ_v is the flexural buckling reduction factor, which should be replaced by χ_{TF} for members where torsional-flexural buckling is critical, while k_{vv} is the interaction factor defined thus:

$$k_{vv} = \begin{cases} 1 + 2.8\left(\bar{\lambda} - 0.5\right) n_v & \text{for} \quad \bar{\lambda} < 1.2 \\ 1 + 1.96 n_v & \text{for} \quad \bar{\lambda} \geqslant 1.2, \end{cases} \tag{8}$$

in which $\bar{\lambda}$ is replaced by $\bar{\lambda}_{TF}$ when torsional-flexural buckling is critical and n_v is given as follows:

$$n_v = \frac{N_{Ed}}{\chi_v N_{Rk}/\gamma_{M1}}. \tag{9}$$

Note that Eq. (8) is specified in prEN 1993-1-4 [44] for I-section members and, in the absence of further guidance, is assumed herein to be also applicable to angles. Comparisons of the test and FE ultimate capacities N_u with the resistances predicted by EC3 $N_{b,EC3}$ are made in Table 9, where a distinction is drawn between the members based on the direction of the applied loading eccentricity. Comparisons are also shown in Fig. 25, where R_u signifies the test/FE ultimate capacity under combined loading, defined thus:

$$R_u = \sqrt{N_u^2 + M_u^2}, \tag{10}$$

and $R_{b,Rd}$ is the resistance under combined loading, given by:

$$R_{b,Rd} = \sqrt{N_{b,Rd}^2 + M_{b,Rd}^2}, \tag{11}$$

with $R_{b,EC3}$ and $R_{b,prop}$ referring to the EC3 [44] and proposed resistances, respectively. The angle θ is illustrated in Fig. 26 and is calculated as:

$$\theta = \arctan\left(\frac{M_u/M_{b,Rd}}{N_u/N_{b,Rd}}\right) = \arctan\left[\frac{N_{b,Rd}(e_0 + e_{N,v})}{M_{b,Rd}}\right]. \tag{12}$$

The EC3 resistance predictions can be seen to be scattered. For cases where the section legs are in compression (see Fig. 25(a)), the scatter of the results is more significant for intermediate to high values of θ, and there are a number of predictions on the unsafe side; this is owing to the fact that lateral–torsional buckling is ignored for the minor-axis bending of angles in the current EC3 guidance [6,7]. On the other hand, an overestimation of the shift of the effective centroid [33] and the loss of effectiveness due to local buckling result in conservative predictions for other cases in the same group of data. For cases where the tips of the cross-section legs are in tension (see Fig. 25(b)), the predicted resistances are generally conservative for low θ values i.e. where axial compression is dominant; this is owing to the double-counting of the same buckling mode (i.e. torsional and local buckling) in EC3 [2–5]. A new interaction curve, anchored to the end points determined on the basis of the new proposals in [6,7], is needed to provide more accurate resistance predictions for pin-ended stainless steel equal-leg angle section members under combined compression and minor-axis bending.

7. New design proposals

Recent proposals for the design of stainless steel equal-leg angle section fixed-ended columns [5] and simply-supported beams [7], along with the expression proposed in [2] for determining the shift of the effective centroid, are adopted in the present paper to develop new proposals for the design of pin-ended stainless steel angle section

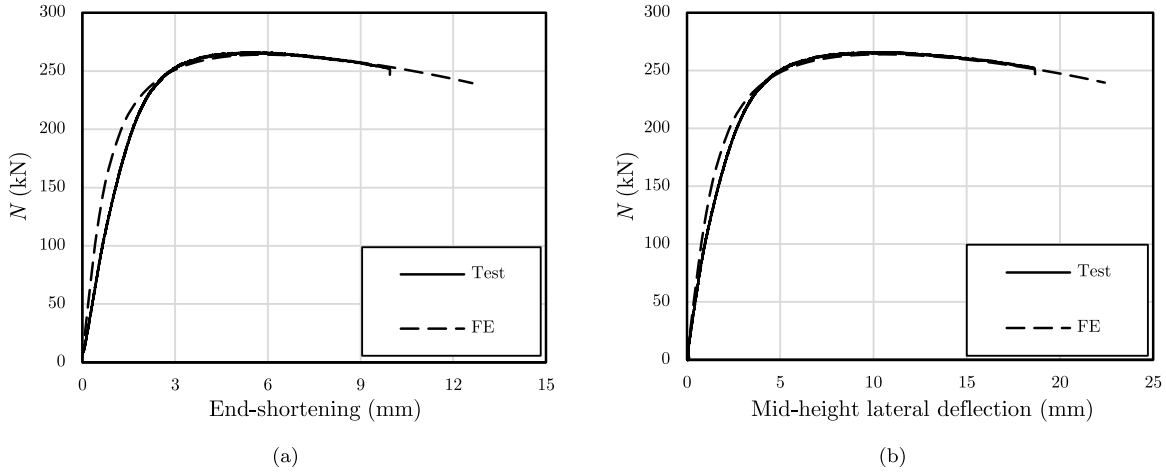

Fig. 21. Comparisons of typical load N versus (a) end-shortening and (b) mid-height lateral displacement curves from a beam–column test and FE model for a specimen (Specimen 11) examined in the present study with $L = 400$ mm and $\omega_g = 36.7$ mm.

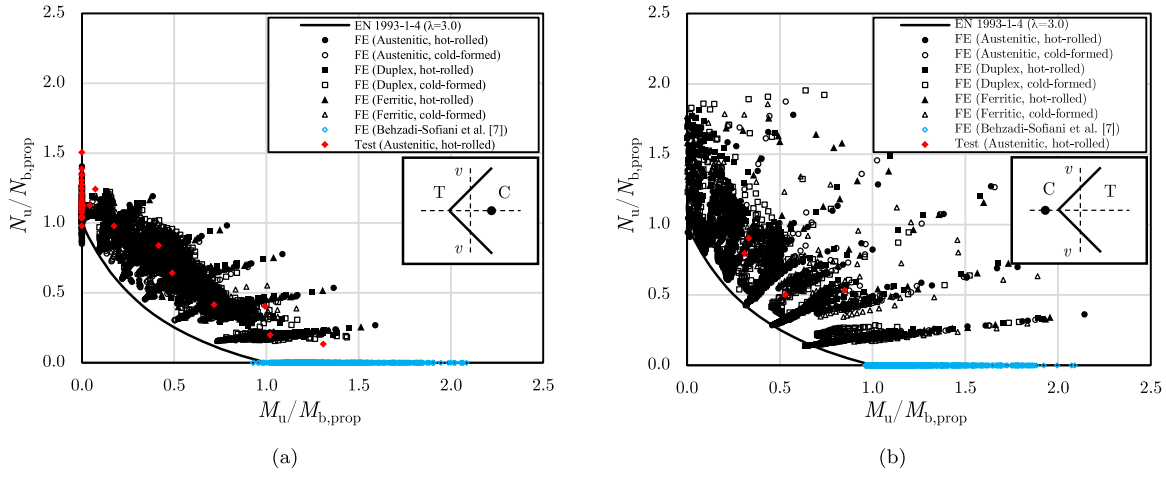

Fig. 22. Comparison of test and FE results for pin-ended stainless steel equal-leg angle section columns and beam–columns bending about the minor axis against EC3 interaction curve for the cases where the loading eccentricities are applied in (a) the positive direction (i.e. the tips of the cross-section legs are in compression) and (b) the negative direction (i.e. the tips of the cross-section legs are in tension).

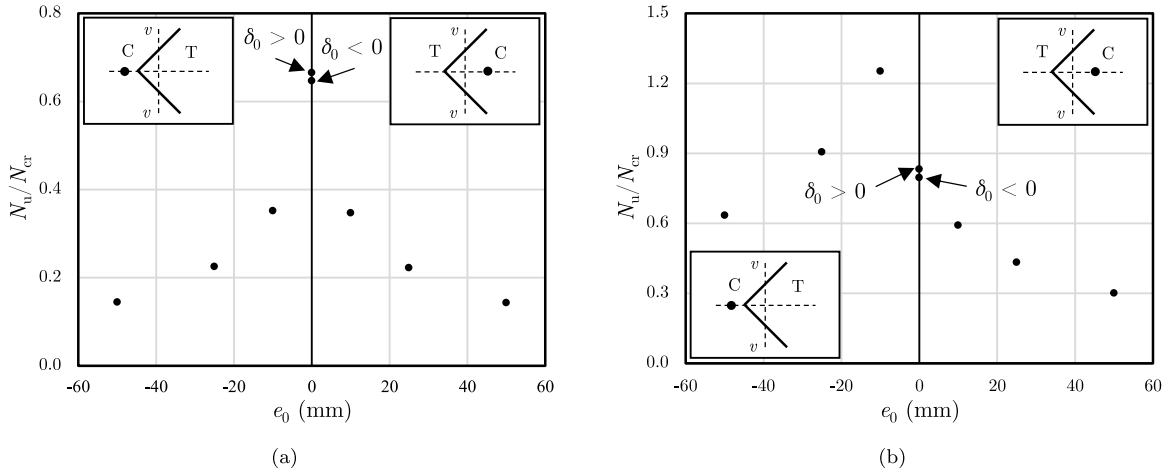

Fig. 23. Variation in normalised ultimate capacity with loading eccentricity for equal-leg angles with (a) $\bar{\lambda}_p = 1.0$ and (b) $\bar{\lambda}_p = 2.0$.

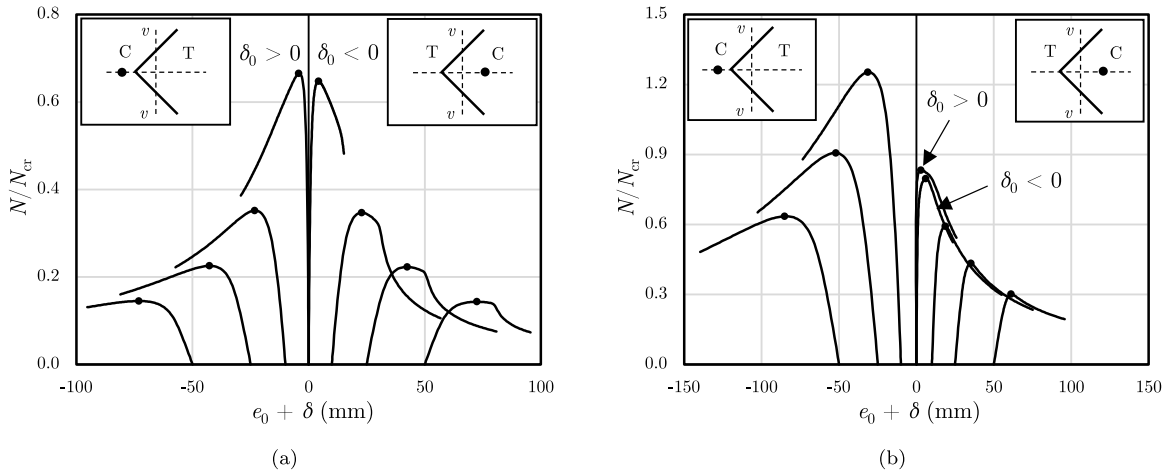

Fig. 24. Equilibrium paths from geometrically and materially nonlinear analyses for equal-leg angles with (a) $\bar{\lambda}_p = 1.0$ and (b) $\bar{\lambda}_p = 2.0$.

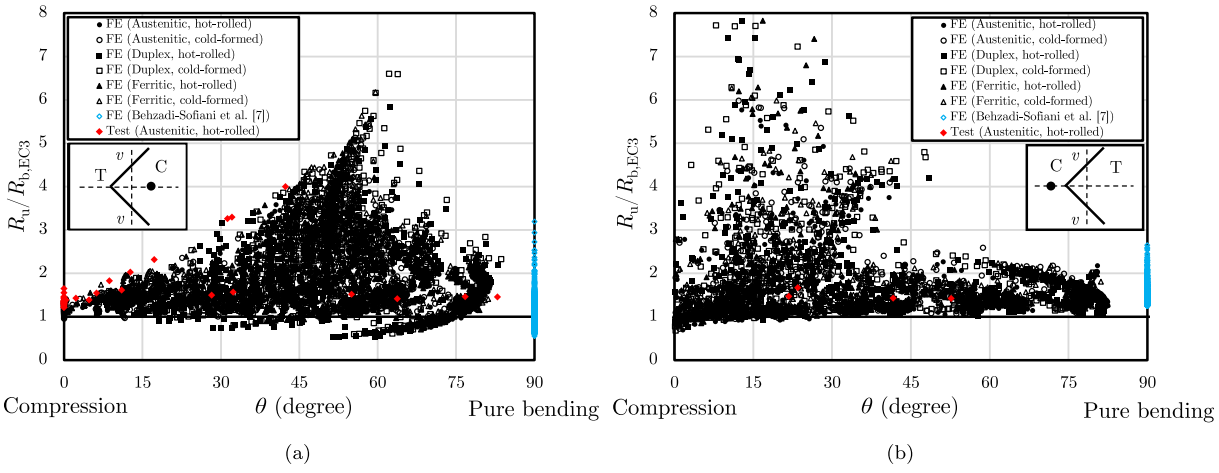

Fig. 25. Comparisons of test and FE results with EC3 ultimate capacities for pin-ended stainless steel equal-leg angle section columns and beam–columns for the cases where the eccentricities are applied in (a) the positive direction (i.e. the tips of the cross-section legs are in compression) and (b) the negative direction (i.e. the tips of the cross-section legs are in tension).

Table 9
Summary of comparisons of test and FE results with EC3 resistance predictions for pin-ended stainless steel equal-leg angle section columns and beam–columns bending about the minor axis.

Source	Manufacturing process	Stainless steel family	Evaluation parameter	$N_u/N_{b,EC3}$		
				Tips in compression	Tips in tension	Total
FE	Hot-rolled	Austenitic	Mean	1.90	1.60	1.76
			CoV	0.42	0.47	0.45
		Duplex	Mean	1.96	1.81	1.89
			CoV	0.47	0.62	0.54
		Ferritic	Mean	1.95	1.70	1.84
			CoV	0.43	0.55	0.48
	Cold-formed	Austenitic	Mean	2.05	1.71	1.90
			CoV	0.46	0.48	0.48
		Duplex	Mean	2.14	1.91	2.03
			CoV	0.50	0.57	0.53
		Ferritic	Mean	2.11	1.75	1.95
			CoV	0.47	0.49	0.49
Test	Hot-rolled	Austenitic	Mean	1.61	1.50	1.60
			CoV	0.38	0.08	0.36

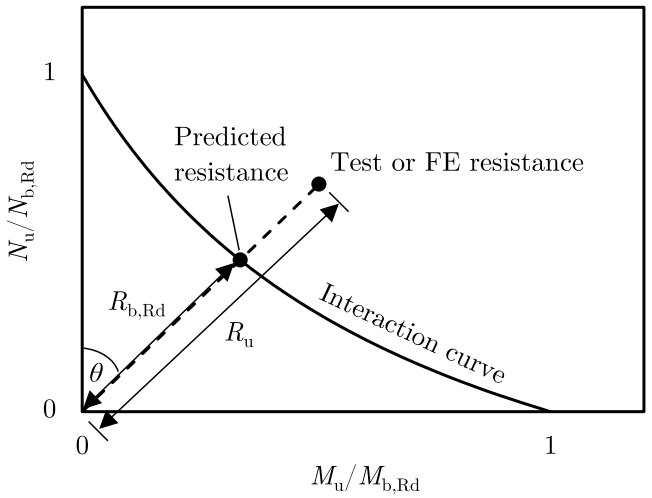

Fig. 26. Definition of parameters R_u, $R_{b,Rd}$ and θ.

columns and beam–columns with bending about the minor axis. The proposed new design formula is given by:

$$\frac{N_{Ed}}{N_{b,Rd}} + k_{vv}\frac{\left(M_{v,Ed} + \Delta M_{v,Ed}\right)}{M_{b,v,Rd}} \leqslant 1.0, \tag{13}$$

where $N_{b,Rd}$ and $M_{b,v,Rd}$ are the member buckling resistances under axial compression and bending about the minor v–v axis, respectively. The new proposals for $N_{b,Rd}$ [5] and $M_{b,v,Rd}$ [7] are summarised in the subsequent subsections.

7.1. Member buckling resistance under axial compression

7.1.1. Torsional-flexural buckling critical (i.e. $N_{cr,TF} \leqslant N_{cr,F,v}$)

The proposed design expression for determining the buckling resistance of stainless steel equal-leg angle section members under compression [5] when torsional-flexural buckling is critical, is given thus:

$$N_{b,Rd} = \frac{\chi_{TF} A f_y}{\gamma_{M1}}, \tag{14}$$

noting that the gross area A is used for all classes of cross-section. In Eq. (14):

$$\chi_{TF} = \chi_F + \Delta_F\left(\chi_T - \chi_F\right) \tag{15}$$

in which the torsional buckling reduction factor χ_T is given by:

$$\chi_T = \frac{\bar{\lambda}_{TF} - 0.188}{\bar{\lambda}_{TF}^2} \quad \text{and} \quad \chi_T \leqslant 1.0 \tag{16}$$

the flexural buckling reduction factor χ_F is given by:

$$\chi_F = \frac{1}{\phi + \sqrt{\phi^2 - \bar{\lambda}_{TF}^2}} \quad \text{and} \quad \chi_F \leqslant 1.0 \tag{17}$$

and Δ_F is given thus:

$$\Delta_F = \left(1 - \frac{N_{cr,TF}}{N_{cr,F,v}}\right)^p \tag{18}$$

where:

$$p = \begin{cases} 2.0\bar{\lambda}_{TF} & \text{for} \quad \bar{\lambda}_{TF} \leqslant 2.0 \\ 2.93\bar{\lambda}_{TF}^{0.45} & \text{for} \quad \bar{\lambda}_{TF} > 2.0 \end{cases} \tag{19}$$

with the torsional-flexural slenderness $\bar{\lambda}_{TF}$ and ϕ being given thus:

$$\bar{\lambda}_{TF} = \sqrt{\frac{A f_y}{N_{cr,TF}}}, \tag{20}$$

$$\phi = 0.5\left[1 + 1.45\alpha\left(\bar{\lambda}_{TF} - 0.2\right)^{1.45} + \bar{\lambda}_{TF}^2\right]. \tag{21}$$

For the imperfection factor α, values of 0.6 and 0.49 are recommended for hot-rolled and cold-formed stainless steel angles, respectively. The value of 0.6 is also used for laser-welded sections in prEN 1993-1-4 [44,48], but could be relaxed to 0.76 if retention of the traditional buckling curves (i.e. curve d in this case) was desirable.

7.1.2. Minor-axis flexural buckling critical (i.e. $N_{cr,F,v} < N_{cr,TF}$)

The proposed design expression for determining the buckling resistance of stainless steel equal-leg angle section members under axial compression [5], when minor-axis flexural buckling is critical is:

$$N_{b,Rd} = \frac{\chi_F A f_y}{\gamma_{M1}} \tag{22}$$

where:

$$\chi_F = \frac{1}{\phi + \sqrt{\phi^2 - \bar{\lambda}^2}} \quad \text{and} \quad \chi_F \leqslant 1.0 \tag{23}$$

in which the normalised slenderness $\bar{\lambda}$ and ϕ are given by:

$$\bar{\lambda} = \sqrt{\frac{A f_y}{N_{cr,F,v}}} \tag{24}$$

$$\phi = 0.5\left[1 + \alpha\beta\left(\bar{\lambda} - 0.2\right)^{\beta} + \bar{\lambda}^2\right] \tag{25}$$

with β being a factor allowing for the influence of interactive (torsional-flexural and minor-axis flexural) buckling:

$$\beta = 1.9 - 0.45\frac{N_{cr,TF}}{N_{cr,F,v}} \quad \text{and} \quad 1.0 \leqslant \beta \leqslant 1.45. \tag{26}$$

The imperfection factor remains as specified above: $\alpha = 0.6$ and $\alpha = 0.49$ for hot-rolled and cold-formed stainless steel angles, respectively.

7.2. Member buckling resistance under minor-axis bending

For determining the member buckling resistance of stainless steel equal-leg angle section members under minor-axis bending, the following expression is proposed [7]:

$$M_{b,v,Rd} = \frac{\chi W_{pl,v} f_y}{\gamma_{M1}} \tag{27}$$

in which the plastic section modulus $W_{pl,v}$ is used for all classes of cross-section. In Eq. (27):

$$\chi = \frac{1}{\phi + \sqrt{\phi^2 - \bar{\lambda}_{max,v}^2}} \quad \text{and} \quad \chi \leqslant 1.0 \tag{28}$$

in which the maximum normalised slenderness $\bar{\lambda}_{max,v}$ and ϕ are given by:

$$\bar{\lambda}_{max,v} = \sqrt{\frac{W_{pl,v} f_y}{M_{cr}}} \tag{29}$$

$$\phi = 0.5\left[1 + 0.13\left(\bar{\lambda}_{max,v} - 0.40\right) + \bar{\lambda}_{max,v}^2\right] \tag{30}$$

where M_{cr} is the minimum of the minor-axis lateral–torsional $M_{cr,LT,v}$ and the Brazier flattening $M_{cr,Br}$ critical buckling moments.

7.3. Interaction factor k_{vv}

The suitability of the existing interaction factor k_{vv} for use with the new proposed end points of the interaction curve (i.e. the axial and bending resistances set out in Sections 7.1 and 7.2) is assessed herein. The expression for the interaction factor k_{vv} takes the general bilinear form given thus:

$$k_{vv} = 1 + \left(D_1\bar{\lambda} + D_2\right)n_v, \tag{31}$$

where D_1 and D_2 are constants. Eq. (31) can be rearranged into the following expression:

$$\frac{k_{vv} - 1}{n_v} = D_1\bar{\lambda} + D_2. \tag{32}$$

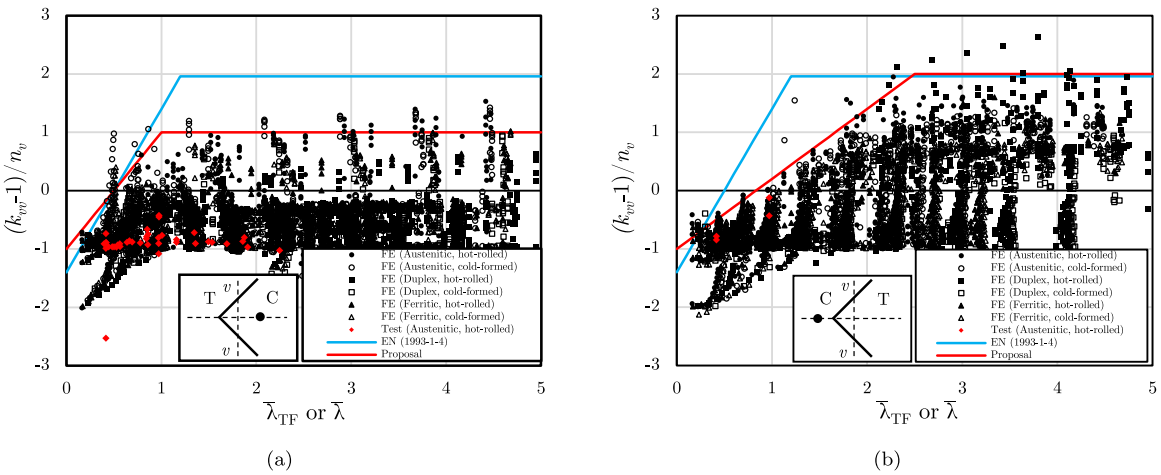

Fig. 27. Comparisons of test and FE results with the existing EC3 and proposed interaction factors k_{vv} for combined compression and bending about the minor axis for the cases where the loading eccentricities are applied in (a) the positive direction (i.e. the tips of the cross-section legs are in compression) and (b) the negative direction (i.e. the tips of the cross-section legs are in tension).

The $(k_{vv}-1)/n_v$ values corresponding to the test and FE results are plotted against the critical normalised slenderness, $\bar{\lambda}_{TF}$ or $\bar{\lambda}$, in Figs. 27(a) and 27(b) for cases with positive and negative initial loading eccentricities, respectively. The bilinear EC3 expression for the interaction factor for I-sections (i.e. $D_1 = 2.8$ and $D_2 = -1.4$ with an upper boundary of 1.96) is also shown, and can be seen to lie generally on the safe side of (i.e. above) the experimental and numerical results, but excessively so. New expressions were therefore sought that provide a closer match to the data [53]; the following expressions are proposed:

$$\text{For tips in compression} \quad k_{vv} = \begin{cases} 1 + \left(2\bar{\lambda} - 1\right) n_v & \text{for} \quad \bar{\lambda} \leqslant 1.0 \\ 1 + n_v & \text{for} \quad \bar{\lambda} > 1.0, \end{cases} \tag{33}$$

$$\text{For tips in tension} \quad k_{vv} = \begin{cases} 1 + \left(1.2\bar{\lambda} - 1\right) n_v & \text{for} \quad \bar{\lambda} \leqslant 2.5 \\ 1 + 2n_v & \text{for} \quad \bar{\lambda} > 2.5. \end{cases} \tag{34}$$

7.4. Assessment of design proposals

A summary of the comparisons of the test and FE capacities with the resistance predictions determined according to the new design proposals $N_{b,prop}$ is presented in Table 10 and Fig. 28. By comparing Figs. 25 and 28, it can be seen that the resistance predictions are significantly improved (noting the substantial difference in the vertical axis scale used in Figs. 25 and 28) for pin-ended stainless steel angles under compression and combined loading using the new proposals relative to the current Eurocode 3 provisions.

7.5. Reliability analysis

The reliability of both the prEN 1993-1-1 [44] and newly proposed design approaches for pin-ended stainless steel equal-leg angle section members subjected to compression and combined loading is evaluated in accordance with [54]. As provided in Afshan et al. [55], the material over-strength factor $f_{y,m}/f_{y,n}$ (i.e. the ratio of the mean to the nominal yield strength) and the corresponding CoV of the yield strength V_{f_y} were taken as 1.3 and 0.06 for austenitic, 1.1 and 0.03 for duplex, and 1.2 and 0.045 for ferritic stainless steel, while the CoV of the Young's modulus was taken as 0.03. The CoV of the cross-sectional area V_A was obtained based on the parameters of the geometric dimensions provided in Annex E of [56] and adopting the procedure outlined in [55], which led to a V_A value equal to 0.03. Following Annex E of [56], the mean values of the Young's modulus and all the geometric properties were taken equal to the nominal values. A summary of the reliability analysis procedure is provided in [4]. The key reliability analysis results are presented in Tables 11 and 12 for the current EC3 rules and the new design proposals, respectively, where the design fractile factor $k_{d,n}$, the CoV of the test and FE resistances relative to the predictions from the resistance model V_δ, and the combined CoV, incorporating the variability of the resistance model and the basic variables V_r, were calculated in accordance with [54]; γ^*_{M1} is the required value of the partial safety factor taken as the mean value for all test and FE results and determined following the approach in [55], while γ_{M1} is the target partial safety factor value (equal to 1.1) and f_a is the acceptance limit [57], given thus:

$$f_a = 1.03 + 0.75(V_r - 0.04) \quad \text{with} \quad 1.03 \leqslant f_a \leqslant 1.15. \tag{35}$$

The ratio $\gamma^*_{M1}/\gamma_{M1}$ should satisfy:

$$\gamma^*_{M1}/\gamma_{M1} \leqslant f_a. \tag{36}$$

A graphical comparison between the obtained $\gamma^*_{M1}/\gamma_{M1}$ values and the acceptance limit f_a is presented in Fig. 29 for the new design method. The current EC3 design expressions clearly lead to unacceptably high γ^*_{M1} values, owing principally to the excessively high scatter of the resistance predictions. On the other hand, the proposed design method leads to $\left(\gamma^*_{M1}/\gamma_{M1}\right)/f_a$ ratios less than 1.0 for both hot-rolled and cold-formed stainless steel members and is therefore considered to satisfy the reliability requirements. Note that, even with the proposed design rules, owing to the relatively high scatter associated with the sensitive buckling response of pin-ended angle section columns and beam–columns compared to, for example, I-section and hollow section [55] members failing by flexural buckling, the mean test/FE to predicted resistance ratios need to be somewhat higher (i.e. higher b values) than is customary in order to satisfy the reliability requirements.

8. Conclusions

A comprehensive study into the behaviour and design of pin-ended stainless steel equal-leg angle section members subjected to compression and combined compression and minor-axis bending has been presented herein. A programme of physical experiments on pin-ended hot-rolled austenitic stainless steel angle section columns and beam–columns, together with supporting material tests and initial geometric imperfection measurements, was first reported. Finite element models were then developed and validated against the reported test results and additional test results from the literature; good agreement between the test and FE results was found. A parametric study was subsequently conducted on both hot-rolled and cold-formed angle section columns and beam–columns in austenitic, duplex and ferritic stainless steel

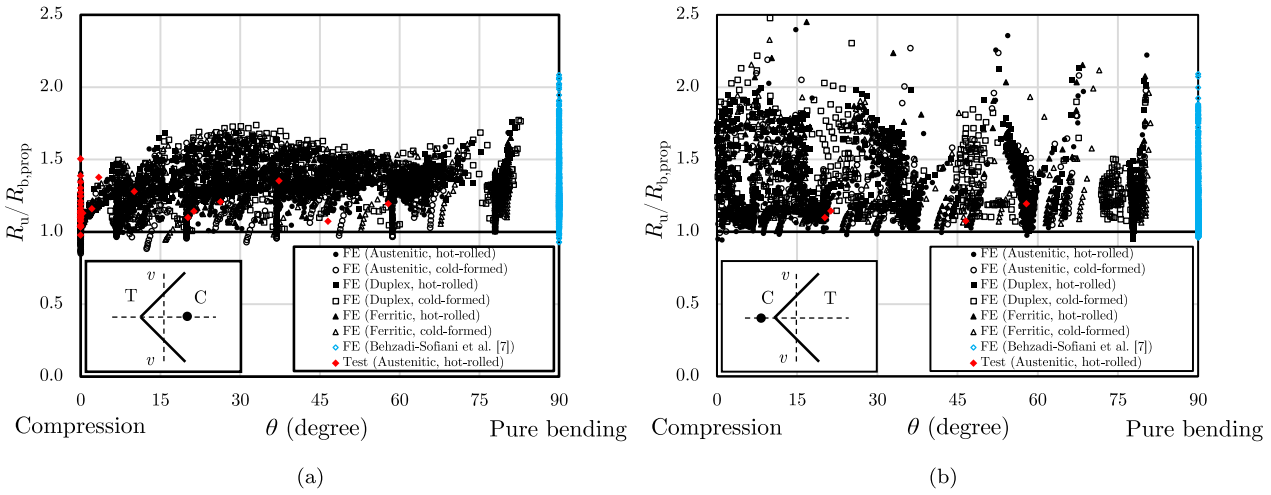

Fig. 28. Comparisons of test and FE results with resistance predictions determined according to the new design proposals for pin-ended stainless steel equal-leg angle section columns and beam–columns for the cases where the loading eccentricities are applied in (a) the positive direction (i.e. the tips of the cross-section legs are in compression) and (b) the negative direction (i.e. the tips of the cross-section legs are in tension).

Table 10
Summary of comparisons of test and FE results with resistance predictions according to the new proposals for pin-ended stainless steel equal-leg angle section columns and beam–columns bending about the minor axis.

Source	Manufacturing process	Stainless steel family	Evaluation parameter	$N_u/N_{b,EC3}$		
				Tips in compression	Tips in tension	Total
FE	Hot-rolling	Austenitic	Mean	1.26	1.24	1.25
			CoV	0.12	0.18	0.15
		Duplex	Mean	1.33	1.34	1.34
			CoV	0.10	0.19	0.14
		Ferritic	Mean	1.29	1.31	1.30
			CoV	0.10	0.20	0.16
	Cold-forming	Austenitic	Mean	1.25	1.27	1.26
			CoV	0.14	0.18	0.16
		Duplex	Mean	1.34	1.37	1.35
			CoV	0.12	0.21	0.17
		Ferritic	Mean	1.29	1.30	1.30
			CoV	0.13	0.17	0.15
Test	Hot-rolling	Austenitic	Mean	1.19	1.13	1.18
			CoV	0.11	0.05	0.11

Table 11
Reliability analysis results for pin-ended stainless steel angle section columns and beam–columns bending about the minor axis for the current EC3 methodology.

Source	Manufacturing process	Stainless steel family	Part in compression	$k_{d,n}$	b	V_δ	V_r	γ^*_{M1}	$\frac{\gamma^*_{M1}}{\gamma_{M1}}$	f_a	$\frac{\gamma^*_{M1}/\gamma_{M1}}{f_a}$
FE	Hot-rolling	Austenitic	Tips	3.098	1.896	0.406	0.411	1.76	1.60	1.15	1.39
			Corner	3.098	1.595	0.377	0.382	1.83	1.67	1.15	1.45
		Duplex	Tips	3.098	1.956	0.480	0.481	2.27	2.06	1.15	1.79
			Corner	3.098	1.812	0.464	0.466	2.30	2.09	1.15	1.82
		Ferritic	Tips	3.098	1.952	0.415	0.418	1.83	1.66	1.15	1.45
			Corner	3.098	1.697	0.399	0.402	1.91	1.74	1.15	1.51
	Cold-forming	Austenitic	Tips	3.098	2.047	0.445	0.449	1.88	1.71	1.15	1.49
			Corner	3.098	1.713	0.388	0.392	1.77	1.61	1.15	1.40
		Duplex	Tips	3.098	2.138	0.501	0.502	2.22	2.02	1.15	1.75
			Corner	3.098	1.907	0.459	0.460	2.15	1.96	1.15	1.70
		Ferritic	Tips	3.098	2.114	0.455	0.457	1.93	1.76	1.15	1.53
			Corner	3.098	1.746	0.385	0.388	1.79	1.63	1.15	1.41
Test	Hot-rolling	Austenitic	Tips	3.334	1.606	0.282	0.287	1.44	1.31	1.15	1.14
			Corner	3.334	1.500	0.076	0.094	0.78	0.71	1.07	0.66

covering a spectrum of cross-section and member geometries and load combinations, with some 7920 numerical results being generated. The FE results, combined with the test results, were used to assess the current EC3 design provisions for pin-ended stainless steel equal-leg angle section columns and beam–columns. The resistance predictions were found to be highly scattered relative to the test and numerical data, with results on both the conservative and unsafe side, depending on the load combination. For column buckling resistance, the current

Table 12
Reliability analysis results for pin-ended stainless steel angle section columns and beam–columns bending about the minor axis for the new design proposals.

Source	Manufacturing process	Stainless steel family	Part in compression	$k_{d,n}$	b	V_δ	V_r	γ^*_{M1}	$\frac{\gamma^*_{M1}}{\gamma_{M1}}$	f_a	$\frac{\gamma^*_{M1}/\gamma_{M1}}{f_a}$
FE	Hot-rolling	Austenitic	Tips	3.098	1.257	0.118	0.135	1.12	1.02	1.10	0.92
			Corner	3.098	1.238	0.164	0.176	1.21	1.10	1.13	0.97
		Duplex	Tips	3.098	1.334	0.096	0.103	1.02	0.93	1.08	0.86
			Corner	3.098	1.340	0.179	0.183	1.25	1.14	1.14	1.00
		Ferritic	Tips	3.098	1.293	0.104	0.116	1.06	0.96	1.09	0.88
			Corner	3.098	1.307	0.174	0.181	1.22	1.11	1.14	0.98
	Cold-forming	Austenitic	Tips	3.098	1.255	0.139	0.154	1.20	1.09	1.12	0.98
			Corner	3.098	1.275	0.167	0.178	1.18	1.08	1.13	0.95
		Duplex	Tips	3.098	1.342	0.118	0.124	1.09	0.99	1.09	0.90
			Corner	3.098	1.369	0.184	0.188	1.26	1.14	1.14	1.00
		Ferritic	Tips	3.098	1.293	0.129	0.139	1.14	1.04	1.10	0.94
			Corner	3.098	1.300	0.159	0.166	1.17	1.06	1.12	0.95
Test	Hot-rolling	Austenitic	Tips	3.334	1.187	0.103	0.119	1.03	0.94	1.09	0.86
			Corner	3.334	1.128	0.047	0.074	0.93	0.85	1.06	0.80

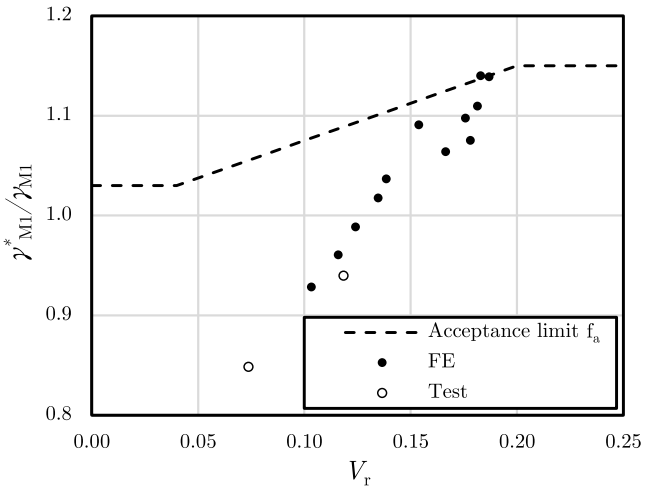

Fig. 29. Comparison of $\gamma^*_{M1}/\gamma_{M1}$ ratios with acceptance limit f_a for new design proposals.

EC3 design provisions account for torsional/local buckling twice, which is the primary source of the observed conservatism. For angles subjected to bending about the minor axis, lateral–torsional buckling can occur, and ignoring this mode of buckling results in unconservative resistance predictions. In addition, the shift of the effective centroid is over-estimated in the current guidance, resulting in a corresponding over-estimation of the minor-axis bending moment. These issues, together with an absence of a specific interaction curve for angle section members, lead to the inaccurate EC3 resistance predictions. A new design approach for pin-ended stainless steel angle section members under compression and combined loading, reflecting the above findings has been proposed. Overall, the new design proposals have been shown to lead to significantly more accurate and reliable resistance predictions for both hot-rolled and cold-formed pin-ended stainless steel equal-leg angle section columns and beam–columns.

CRediT authorship contribution statement

Behnam Behzadi-Sofiani: Conceptualization, Investigation, Formal analysis, Methodology, Validation, Writing – original draft. **M. Ahmer Wadee:** Conceptualization, Methodology, Supervision, Writing – review & editing. **Leroy Gardner:** Conceptualization, Methodology, Supervision, Writing – review & editing.

Declaration of competing interest

The authors declare that they have no known competing financial interests or personal relationships that could have appeared to influence the work reported in this paper.

Data availability

Data will be made available on request.

Acknowledgements

The authors would like to thank Dr Barbara Rossi for the acquisition of the test material and gratefully acknowledge the financial support of the Skempton scholarship from Imperial College London, United Kingdom.

References

[1] A.H. Stang, L.R. Strickenberg, Results of Some Compression Tests of Structural Steel Angles, US Government Printing Office, 1922.
[2] K.J.R. Rasmussen, Design of angle columns with locally unstable legs, J. Struct. Eng. 131 (10) (2005) 1553–1560.
[3] P.B. Dinis, D. Camotim, A novel DSM-based approach for the rational design of fixed-ended and pin-ended short-to-intermediate thin-walled angle columns, Thin-Walled Struct. 87 (2015) 158–182.
[4] B. Behzadi-Sofiani, L. Gardner, M.A. Wadee, P.B. Dinis, D. Camotim, Behaviour and design of fixed-ended steel equal-leg angle section columns, J. Constr. Steel Res. 182 (2021) 106649.
[5] B. Behzadi-Sofiani, L. Gardner, M.A. Wadee, Stability and design of fixed-ended stainless steel equal-leg angle section columns, Eng. Struct. 249 (2021) 113281.
[6] B. Behzadi-Sofiani, L. Gardner, M.A. Wadee, Testing, simulation and design of steel equal-leg angle section beams, Thin-Walled Struct. 171 (2022) 108698.
[7] B. Behzadi-Sofiani, L. Gardner, M.A. Wadee, Testing, numerical analysis and design of stainless steel equal-leg angle section beams, Structures 37 (2022) 977–1001.
[8] P. Dinis, D. Camotim, Buckling, post-buckling and strength of equal-leg angle and cruciform columns: Similarities and differences, in: A.L. Dunai, M. Iványi, K. Jármai, N. Kovács, L.G. Vigh (Eds.), Proc. 6th European Conf. on Steel and Composite Structures, EUROSTEEL, in: European Convention for Constructional Steelwork, Brussels, Belgium, 2011, pp. 105–110.
[9] A. Landesmann, D. Camotim, P.B. Dinis, R. Cruz, Short-to-intermediate slender pin-ended cold-formed steel equal-leg angle columns: Experimental investigation, numerical simulations and DSM design, Eng. Struct. 132 (2017) 471–493.
[10] EN 1993-1-4, Eurocode 3: Design of Steel Structures – Part 1-4: General Rules – Supplementary Rules for Stainless Steels, European Committee for Standardisation (CEN), Brussels, Belgium, 2006.
[11] A.A. de Menezes, P.C.da S. Vellasco, L.R. de Lima, A.T. da Silva, Experimental and numerical investigation of austenitic stainless steel hot-rolled angles under compression, J. Construct. Steel Res. 152 (2019) 42–56.
[12] Y. Liang, V.V.K. Jeyapragasam, L. Zhang, O. Zhao, Flexural–torsional buckling behaviour of fixed-ended hot-rolled austenitic stainless steel equal-leg angle section columns, J. Construct. Steel Res. 154 (2019) 43–54.

[13] Y. Sun, Z. Liu, Y. Liang, O. Zhao, Experimental and numerical investigations of hot-rolled austenitic stainless steel equal-leg angle sections, Thin-Walled Struct. 144 (2019) 106225.
[14] F. Sarquis, L. de Lima, P.da S. Vellasco, M. Rodrigues, Experimental and numerical investigation of hot-rolled stainless steel equal leg angles under compression, Thin-Walled Struct. 151 (2020) 106742.
[15] A.da S. Sirqueira, P.da S. Vellasco, L. de Lima, F. Sarquis, Experimental assessment of stainless steel hot-rolled equal legs angles in compression, J. Construct. Steel Res. 169 (2020) 106069.
[16] A. Filipović, J. Dobrić, N. Baddoo, P. Može, Experimental response of hot-rolled stainless steel angle columns, Thin-Walled Struct. 163 (2021) 107659.
[17] A. Filipović, J. Dobrić, D. Budevac, N. Fric, N. Baddoo, Experimental study of laser-welded stainless steel angle columns, Thin-Walled Struct. 164 (2021) 107777.
[18] L. Zhang, K.H. Tan, O. Zhao, Experimental and numerical studies of fixed-ended cold-formed stainless steel equal-leg angle section columns, Eng. Struct. 184 (2019) 134–144.
[19] L. Zhang, K.H. Tan, O. Zhao, Local stability of press-braked stainless steel angle and channel sections: Testing, numerical modelling and design analysis, Eng. Struct. 203 (2020) 109869.
[20] J. Dobrić, A. Filipović, Z. Marković, N. Baddoo, Structural response to axial testing of cold-formed stainless steel angle columns, Thin-Walled Struct. 156 (2020) 106986.
[21] N.A. Reynolds, Behavior and Design of Concentrically Loaded Duplex Stainless Steel Single Equal-Leg Angle Struts (Ph.D. thesis), Georgia Institute of Technology, 2013.
[22] L. Zhang, Y. Liang, O. Zhao, Experimental and numerical investigations of pin-ended hot-rolled stainless steel angle section columns failing by flexural buckling, Thin-Walled Struct. 156 (2020) 106977.
[23] L. Zhang, Y. Liang, O. Zhao, Laboratory testing and numerical modelling of pin-ended hot-rolled stainless steel angle section columns failing by flexural–torsional buckling, Thin-Walled Struct. 161 (2021) 107395.
[24] J. Dobrić, A. Filipović, N. Baddoo, Z. Marković, D. Budevac, Design procedures for cold-formed stainless steel equal-leg angle columns, Thin-Walled Struct. 159 (2021) 107210.
[25] J. Dobrić, A. Filipović, N. Baddoo, D. Budevac, B. Rossi, Design criteria for pin-ended hot-rolled and laser-welded stainless steel equal-leg angle columns, Thin-Walled Struct. 167 (2021) 108175.
[26] J. Dobrić, A. Filipović, N. Baddoo, Z. Marković, D. Budevac, The new buckling curves for cold-formed stainless steel equal-leg angle columns, in: ASES International Congress Proceedings/Association of Structural Engineers of Serbia, 16th Congress, Univerzitet u Beogradu Gradevinski fakultet, 2021, pp. 501–510.
[27] M. Theofanous, A. Liew, L. Gardner, Experimental study of stainless steel angles and channels in bending, Structures 4 (2015) 80–90.
[28] SEI/ASCE 8-02, Specification for the Design of Cold-Formed Stainless Steel Structural Members, American Society of Civil Engineers, 2002.
[29] AS/NZS 4673, Cold-Formed Stainless Steel Structures, Australian/New Zealand Standard, Sydney, 2001.
[30] P.B. Dinis, D. Camotim, N. Silvestre, On the local and global buckling behaviour of angle, T-section and cruciform thin-walled members, Thin-Walled Struct. 48 (10–11) (2010) 786–797.
[31] AISI, North American Specification for the Load and Resistance Factor Design of Cold-Formed Steel Structural Members, Amewrican Iron and Steel Institure (AISI), Washington, 2000.
[32] AS/NZ4600, Design of Cold-Formed Structures, Australian Steel Instiute (ASI), Australia, Sydney, 1996.
[33] EN 1993-1-5, Eurocode 3: Design of Steel Structures – Part 1-5: Plated Structural Elements, European Committee for Standardisation (CEN), Brussels, Belgium, 2006.
[34] EN ISO 6892-1:2019, Metallic Materials – Tensile Testing – Part 1: Method of Test At Room Temperature, European Committee for Standardisation (CEN), Brussels, Belgium, 2019.
[35] E. Mirambell, E. Real, On the calculation of deflections in structural stainless steel beams: an experimental and numerical investigation, J. Construct. Steel Res. 54 (1) (2000) 109–133.
[36] I. Arrayago, E. Real, L. Gardner, Description of stress–strain curves for stainless steel alloys, Mater. Des. 87 (2015) 540–552.
[37] L. Gardner, X. Yun, Description of stress–strain curves for cold-formed steels, Constr. Build. Mater. 189 (2018) 527–538.
[38] X. Yun, Z. Wang, L. Gardner, Full-range stress–strain curves for aluminum alloys, J. Struct. Eng. 147 (6) (2021) 04021060.
[39] L. Gardner, M. Ashraf, Structural design for non-linear metallic materials, Eng. Struct. 28 (6) (2006) 926–934.
[40] C. Kyprianou, P. Kyvelou, L. Gardner, D.A. Nethercot, Experimental study of sheathed cold-formed steel beam–columns, Thin-Walled Struct. 166 (2021) 108044.
[41] H. Beer, G. Schulz, Bases théoriques des courbes européennes de flambement, Constr. Mét. 3 (1970) 37–57.
[42] F. Walport, L. Gardner, D. Nethercot, Equivalent bow imperfections for use in design by second order inelastic analysis, Structures 26 (2020) 670–685.
[43] X. Meng, L. Gardner, Flexural buckling of normal and high strength steel CHS columns, Structures 34 (2021) 4364–4375.
[44] prEN 1993 1-4, Eurocode 3: Design of Steel Structures – Part 1-4: General Rules – Supplementary Rules for Stainless Steels, final document, European Committee for Standardisation (CEN), Brussels, Belgium, 2020.
[45] ABAQUS, Version 6.16 Analysis User's Guide, Dassault Systemes Simulia Corporation, Providence, USA, 2016.
[46] M. Theofanous, T.M. Chan, L. Gardner, Flexural behaviour of stainless steel oval hollow sections, Thin-Walled Struct. 47 (6–7) (2009) 776–787.
[47] M. Kucukler, L. Gardner, L. Macorini, Lateral–torsional buckling assessment of steel beams through a stiffness reduction method, J. Construct. Steel Res. 109 (2015) 87–100.
[48] Y. Bu, L. Gardner, Finite element modelling and design of welded stainless steel i-section columns, J. Construct. Steel Res. 152 (2019) 57–67.
[49] E. Riks, An incremental approach to the solution of snapping and buckling problems, Int. J. Solids Struct. 15 (7) (1979) 529–551.
[50] S. Afshan, O. Zhao, L. Gardner, Standardised material properties for numerical parametric studies of stainless steel structures and buckling curves for tubular columns, J. Construct. Steel Res. 152 (2019) 2–11.
[51] M. Jandera, L. Gardner, J. Machacek, Residual stresses in cold-rolled stainless steel hollow sections, J. Construct. Steel Res. 64 (11) (2008) 1255–1263.
[52] F. Walport, M. Kucukler, L. Gardner, Stability design of stainless steel structures, J. Struct. Eng. 148 (1) (2022) 04021225.
[53] X. Meng, L. Gardner, Testing, modelling and design of normal and high strength steel tubular beam–columns, J. Construct. Steel Res. 183 (2021) 106735.
[54] EN 1990, Eurocode – Basis of Structural Design, European Committee for Standardisation (CEN), Brussels, Belgium, 1990.
[55] S. Afshan, P. Francis, N. Baddoo, L. Gardner, Reliability analysis of structural stainless steel design provisions, J. Construct. Steel Res. 114 (2015) 293–304.
[56] EN 1990, Eurocode 3: Design of Steel Structures – Part 1-1: General Rules and Rules for Buildings, Final Document, European Committee for Standardisation (CEN), Brussels, Belgium, 2019.
[57] L.S. da Silva, T. Tankova, L. Marques, C. Rebelo, A. Taras, Standardisation of Safety Assessment Procedures Across Brittle to Ductile Failure Modes, Final Document, SAFEBRICTILE, European Commission, Directorate-General for Research and Innovation, 2018.